Single Domain Antibody Inhibitors Target the Coiled Coil Arms of the *Bacillus subtilis* SMC complex

Ophélie Gosselin[1], Michael Taschner[1], Lea M. Huber-Hürlimann[2], Markus A. Seeger[2] and Stephan Gruber[1]*

[1]Department of Fundamental Microbiology (DMF), Faculty of Biology and Medicine (FBM), University of Lausanne (UNIL), 1015 Lausanne, Switzerland

[2]Institute of Medical Microbiology, University of Zurich, Zürich, Switzerland

*Corresponding Author: stephan.gruber@unil.ch

Key words: Single domain antibodies, Sybodies, nanobodies, SMC complex, bacterial condensin, DNA loop extrusion, chromosome segregation

Abstract

Synthetic nanobodies—also called sybodies—have proven valuable for stabilizing conformations of purified proteins, advancing structural and functional studies for example of transmembrane protein complexes. However, their utility in modulating protein function in living cells has remained less well explored. Structural Maintenance of Chromosomes (SMC) complexes facilitate chromosome organization by DNA loop extrusion, a fundamental process in all domains of life. In this study, we target the bacterial SMC complex, Smc-ScpAB, in *Bacillus subtilis* with synthetic nanobodies, aiming to identify key functional regions of the protein complex in a largely unbiased manner. We first isolate sybodies that specifically bind purified Smc-ScpAB and then express them in *B. subtilis* to select binders capable of disrupting Smc-ScpAB function, leading to chromosome segregation defects and cell death. Mapping and biochemical characterization show that the fourteen disruptive sybodies belong to one of three library designs, target the Smc subunit near the same coiled coil arm interface and modulate its ATPase activity in two principal ways, highlighting the mid-region of the Smc coiled coil as critical feature of the DNA folding process. These findings underscore the potential of sybodies—and, by extension, designed binders—as versatile tools for probing dynamic protein function in living cells, with potentially broad applications in cell and synthetic biology.

30 **Introduction**

31 Rapid and specific interference with protein activity and dynamics in living cells is essential for studying
32 and understanding biological mechanisms. However, current approaches—primarily based on small-
33 molecule inhibitors—remain laborious, time-consuming, and costly. The advent of conformation-
34 specific synthetic nanobody (sybody) selection [1], and more recently, computational design of protein
35 binders [2], offer unique opportunities for protein-based inhibition and modulation of cellular targets.
36 Here, we generate sybodies against the SMC complex in *B. subtilis* to efficiently inhibit its function
37 within cells.

38 Structural Maintenance of Chromosomes (SMC) complexes are multi-subunit, ring-shaped ATP-
39 hydrolyzing DNA motors that structure chromosomal DNA by loop extrusion. They are essential for
40 chromosome organization and segregation, gene expression, DNA repair, and defense against non-self
41 DNA across all domains of life [3]. Each SMC protein (Smc in *B. subtilis, bsu*Smc) is a long polypeptide
42 with its N- and C-termini folding together to form a globular ATP binding cassette (ABC) "head" domain.
43 The head is connected to a "hinge" dimerization domain via a ~50 nm antiparallel coiled coil "arm",
44 creating an elongated dimer (Figure 1Aii and 1Aiii). ATP binding promotes head engagement, bringing
45 the heads together to form a functional ATPase. Non-SMC subunits, a kleisin (ScpA in *B. subtilis*) and a
46 dimer of KITE (ScpB in *B. subtilis*) or two HAWK proteins, bridge the heads, together forming a ring
47 around DNA (Figure 1Aiii). In *B. subtilis*, Smc-ScpAB is recruited to the origin of replication (*oriC*) region
48 on the chromosome by ParB, a DNA-binding protein that recognizes centromere-like *parS* sequences
49 (Figure 2Ai). Once loaded, Smc-ScpAB translocates at a rate of ~1 kb/s onto flanking DNA, aligning the
50 two chromosome arms and individualizing nascent sister chromosomes[4-6], likely bypassing obstacles
51 on the chromosome through the SMC hinge gate [7]. Null mutants of *smc*, *scpA*, or *scpB* fail to segregate
52 chromosomes properly and lose viability under conditions promoting rapid growth[5,6,8].

53 Several models have been proposed for the mechanism of DNA loop extrusion by SMC complexes,
54 including the "segment capture" model, in which DNA segments are transiently trapped between the

55 SMC arms in partially open states and fused into larger loops through iterative ATP-driven cycles (Figure
56 1Aiii and S1B) [9-11]. However, detailed structural understanding and experimental testing *in vivo* are
57 lacking.

58 Antibodies can block biochemical reactions by stabilizing reaction intermediates. Synthetic single-
59 domain antibodies called sybodies are small, robust antigen-binding proteins that were engineered
60 based on three camelid nanobody structures [1]. They are selected from synthetic libraries that encode
61 a wide diversity of binding surfaces and epitope shapes based on the length and geometry of their
62 CDR3 loop, allowing strong binding of diverse antigen surfaces (Figure 1Ai). Their small size (~15 kDa),
63 stability, and ability to bind transient epitopes make them ideal tools for targeting specific states of
64 biomolecules [12]. Selection is carried out using purified and immobilized Smc-ScpAB by ribosome display
65 and phage display, typically followed by an ELISA-based screening [1].

66 Here, we demonstrate that sybodies can be used to interfere with the function of *B. subtilis* Smc-ScpAB
67 *in vivo*. We first isolate binders that specifically target purified Smc-ScpAB *in vitro* and then select those
68 that eliminate Smc function when expressed in *B. subtilis*. Fourteen sybodies were found to disrupt
69 chromosome segregation, mimicking *smc* deletion phenotypes. Biochemical assays confirmed that
70 selected sybodies alter the ATP hydrolysis rate of Smc-ScpAB and its stimulation by DNA addition, likely
71 stabilizing intermediates of the conformational cycle. Mapping experiments using chimeric Smc
72 constructs revealed that most binders, unexpectedly, target the coiled coil, specifically in a defined
73 region near the Smc 4N arm-to-arm contact [13], highlighting the potential of sybodies and designed
74 binders, as genetic tools to identify essential functional domains and underscoring the importance of
75 coiled coil dynamics for Smc function.

76

77 **Results**

78 **Generation of *bsuS*mc-ScpAB-specific sybodies**

79 To isolate sybodies that impede the function of *B. subtilis* Smc-ScpAB complex, we first performed *in*
80 *vitro* selection with purified Smc-ScpAB in the presence of 40 bp duplex DNA, and an ATPase-deficient
81 mutant (E1118Q) of *bsuS*mc. These conditions favour ATP-engaged complexes alongside the typically
82 predominant ATP-disengaged rod-shaped state [13]. *bsuS*mc was also biotinylated at the hinge at residue
83 R643C for immobilization (Figure 1Aii-iii and S1A) [1,14-16]. Starting from three synthetic sybody libraries
84 encoding distinct epitope-binding geometries (denoted as concave, loop, convex, respectively, Figure
85 1Ai), we performed one round of ribosome display starting from a large sybody library followed by two
86 rounds of phage display, thereby enriching sybodies that bind to Smc-ScpAB (Table 1). From each
87 library, 95 sybody-expressing *E. coli* clones were randomly chosen for *in vivo* characterization. ELISA
88 data revealed that nearly all clones bind purified Smc-ScpAB (Table 1). However, the ELISA signals of
89 only few Sybodies showed clear dependence on the presence or absence of ATP and DNA (Table S1).

90

91 **Identification of *bsuS*mc-ScpAB-blocking sybodies through phenotypic screening in *B. subtilis***

92 We therefore decided to screen for inhibiting sybodies directly in *B. subtilis* cells. Despite containing a
93 conserved disulfide bond, sybodies have been successfully expressed inside cells and were shown to
94 bind their targets in the reducing environment of the cytoplasm, likely owing to their robust folding [17].
95 To assess whether the selected sybodies interfere with Smc function *in vivo*, each of the 285 sybody
96 sequences was cloned under a xylose-inducible promoter (P_{xyl}) into an *E. coli–B. subtilis* shuttle vector
97 and integrated at the *amyE* locus of the wild-type 1A700 strain (Figure 1B) [18]. Fourteen sybodies from
98 the loop library failed to yield transformants in the presence (but not absence) of xylose, indicating cell
99 lethality due to sybody inhibition of Smc-ScpAB (Figure 1C, S2A-B). These Smc-disruptive sybodies
100 (denoted as Sb002, 003, 006, 010, 015, 020, 021, 031, 156, 160, 162, 169, 188, and 194, respectively)
101 harbor fourteen distinct sequences(Table S2). Intriguingly, no such disruptive sybodies were isolated

102 from the concave and convex libraries (Figure S2B), suggesting that the CDR3 geometry as present in
103 the loop library is particularly effective at inhibiting *bsuS*mc-ScpAB. Likely, sybodies of the other
104 libraries bound to other epitopes of *bsuS*mc-ScpAB that are not sensitive to conformational trapping,
105 and it is further possible that they were not stably expressed in *B. subtilis*. However, at least for sybodies
106 from the loop library, we did not notice any obvious correlation between expression levels and
107 phenotypes. Selected sybodies showed similar expression and were appreciably expressed even
108 without inducer (Figure S4, S5). Notably, tendencies of preferential isolation of binders from one of the
109 three libraries have previously been observed, although at milder levels [1,17,19].

110

111 **Selected sybodies target *bsuS*mc-ScpAB function *in vivo***

112 To determine whether the fourteen sybodies indeed impair chromosome segregation, we used
113 fluorescence microscopy to monitor *oriC* positioning in a *B. subtilis* strain expressing a ParB-GFP fusion
114 protein together with a P_{xyl}-inducible sybody gene. In these strains, ParB-GFP marks the replication
115 origin region by binding to *parS* sites near *oriC* (Figure 2Ai). As expected, the *Δsmc* strain displayed
116 fewer ParB-GFP foci and elongated cells (Figure 2Ai) (Table S3). These elongated cells are known to
117 harbour expanded nucleoids, consistent with delayed *oriC* separation rather than delayed DNA
118 replication [6,20]. A time course experiment using sybody Sb006 revealed chromosome organization
119 defects as early as 30 minutes post induction, with a significant reduction in ParB-GFP foci per µm cell
120 length at 40 minutes (p = 0.0145) (Figure 2Aii). Subsequent imaging was performed ~35 minutes after
121 induction of sybody expression.

122 All disruptive sybodies reduced ParB-GFP foci density compared to the control (1.03 foci/µm), with
123 values ranging from 0.56 foci/µm (Sb020) to 0.22 foci/µm (Sb003). These defects were all robustly
124 detected, while being less severe than the Δ*smc* mutant (~0.05 foci/µm), conceivably due to the short
125 induction time or incomplete inhibition. Milder defects were also observed without induction, likely
126 attributed to leaky expression from the P_{xyl} promoter (Figure S3A). Sybody expression also caused cell

127 elongation and growth delays, both hallmarks of impaired Smc activity, consistent with chromosome
128 segregation defects that delay cell division (Figure S3B–C). Altogether, these results show that all
129 selected sybodies induce *Δsmc*-like phenotypes likely by interfering with *bsu*Smc-ScpAB activity *in vivo*.

130

131 **Selected sybodies specifically target *B. subtilis* Smc-ScpAB**

132 To test whether sybodies specifically target *B. subtilis* Smc-ScpAB, we assessed their effects in a strain
133 expressing *Streptococcus pneumoniae* (*Spn*) Smc-ScpAB and ParB proteins in place of the endogenous
134 *B. subtilis* proteins. The *Spn* sequences can functionally replace the corresponding *Bsu* sequences
135 despite significant sequence divergence (~38% sequence identity) [21]. Strikingly, none of the sybodies
136 impaired growth in this background, even though a cognate ParAB pair is absent in this strain (*S.*
137 *pneumoniae* lacks *parA*), sensitizing cells to chromosome segregation defects (Figure 2C). These results
138 confirm that the sybodies are specific to *bsu*Smc-ScpAB and that off-target toxicity is not noticeable.

139

140 ***bsuS*mc-ScpAB-disrupting sybodies target two distinct coiled coil regions adjacent to the *bsuS*mc 4N**
141 **arm-to-arm contact**

142 To map the sybody-binding site on the *bsuS*mc-ScpAB complex, we utilized five chimeric Smc constructs
143 (Smc Chimera 1-5), in which the hinge and progressively longer segments of the adjacent coiled coils
144 were replaced with the corresponding sequences from the *S. pneumoniae* Smc protein (Figure 3A).
145 Chimeric junctions were designed to preserve coiled coil integrity based on available crystal structures,
146 coiled coil predictions by DeepCoil, and AlphaFold2 structural models [1,22,23]. All chimeric Smc strains
147 retained the native *B. subtilis scpA*, *scpB*, and *parB* genes and were viable under conditions promoting
148 fast growth, demonstrating proper protein folding and functioning of chimeric Smc-ScpAB complexes
149 (Figure S6A).

150 Chimeras 1 and 2, which carry the central hinge and coiled coil sequences of *Spn* origin (residues 363-
151 812 and 339-836, respectively), showed the same sybody-induced growth defects as the wild-type
152 strain, indicating that the sybodies bind further away from the hinge, within the remaining *B. subtilis*
153 portion comprising of the Smc head and the first ~230 coiled coil residues, and ScpAB (Figure 3A). By
154 contrast, Chimera 5 (residues 248–927 of *Spn* origin), supported robust growth even in the presence of
155 the *bsu*Smc-disrupting sybodies, indicating that the region comprising the heads and first ~50 residues
156 of the coiled coil (including the joint) does not comprise the binding site. The binding region for the
157 sybodies is thus located on the coiled coil between residues 248 and 339 (or 836 and 927),
158 demonstrating that all fourteen sybodies bind to a central region of the coiled coil.

159 Chimera 3 (*spn*Smc residues 318-857) and chimera 4 (*spn*Smc residues 276-899) revealed two distinct
160 sybody responses. Sb003, 031, 156, 160, 162, and 169 impaired growth of both strains, mapping their
161 binding sites to *B. subtilis* residues 248-276 (and 899-927), present in chimeras 1–4 but absent in
162 chimera 5. In contrast, Sb002, 006, 010, 015, 020, 021, 188, and 194 had no impact on the viability of
163 chimera 3 or 4, suggesting they target residues 318-339/836-857 (Figure 3A, 3D).

164 In sum, these experiments mapped the binding sites of all fourteen disruptive sybodies to one of two
165 ~twenty amino acid segments in the central region of the *bsuS*mc coiled coil (Figure 3D). These regions
166 harbor relatively poorly conserved sequences but flank the 4N arm-arm contact (~at residue 295),
167 previously proposed to serve as an essential structural switch between closed and open
168 conformations[13]. These results reveal that all isolated sybodies target the same functional element of
169 the Smc arms, and that interfering with this element disrupts Smc-dependent chromosome
170 organization *in vivo*.

171

172 **Smc-disrupting sybodies affect the ATPase activity in one of two ways**

173 To investigate how sybodies may influence *bsuS*mc-ScpAB, we next measured ATP hydrolysis rates using
174 purified proteins in the presence and absence of DNA. SMC ATPase activity serves as an indirect

175 readout for state transitions, including arm opening and head engagement. In absence of DNA, *bsuS*mc-
176 ScpAB hydrolyzes ATP at ~4 ATP/min/Smc [13]. DNA binding stimulates ATP hydrolysis to ~9 ATP/min/Smc,
177 presumably by DNA binding promoting arm opening and head engagement, creating a more open
178 conformation.

179 All disruptive sybodies measurably affected the ATP hydrolysis rate of *bsuS*mc-ScpAB. Ten maintained
180 a near-basal ATPase rate even in presence of DNA (Sb002, Sb003, Sb010, Sb031, Sb156, Sb160, Sb162,
181 Sb169, Sb188, and Sb194) (Figure 3B-C and S6B). This suggests that they stabilize the complex in a
182 closed or partially closed conformation, thus hindering DNA-dependent ATPase stimulation. Notably,
183 in this group, Sb002 and Sb194 showed slightly elevated ATPase rates with DNA, hinting at a mildly
184 more flexible conformation.

185 In contrast, the other sybodies (Sb006, Sb015, Sb020, and Sb021) stimulated ATP hydrolysis in the
186 absence of DNA, with Sb006 reaching levels comparable to DNA-induced activation (~10 ATP/min). This
187 implies that these sybodies stabilize Smc-ScpAB in a more open state promoting head engagement.
188 Curiously, addition of DNA in the presence of Sb006 and Sb021 reduced—rather than stimulated—
189 ATPase activity (Figure 3B-C), suggesting that concurrent DNA and sybody binding may trap the complex
190 in a non-productive conformation, perhaps by favoring the open state excessively. These findings are
191 consistent with the idea that 4N contact region plays a critical role in arm opening and ATPase
192 stimulation.

193 Interestingly, the observed ATPase profiles correlate with distinct binding regions along the Smc arms.
194 All ATPase-stimulating sybodies (Sb006, Sb015, Sb020, Sb021) bind above the 4N contact
195 ("Opening^{UP}"), while sybodies that hinder DNA stimulation fall into two subgroups: those binding above
196 the 4N contact (Sb002, Sb010, Sb188, Sb194—"Closing^{UP}") and those binding below it (Sb003, Sb031,
197 Sb156, Sb160, Sb162, Sb169—"Closing^{DOWN}") (Figure 3D). These results indicate that the sybodies
198 perturb *bsuS*mc-ScpAB in two principal ways: either by favoring the opening of the arms or by
199 constraining the arms in a more closed state. The results highlight arm opening and closure as central

200 regulatory features of bacterial Smc-ScpAB [9,11,24,25] and confirm the key role of the 4N arm contact in

201 balancing the opening and closing of SMC arms [13].

202 **Discussion**

203 Over the past three decades, nanobodies and their synthetic counterparts have transformed
204 biomedical research and structural biology by enabling the targeting and stabilization of transient
205 protein conformations. Despite these advances, their application to probing protein function in living
206 cells has remained limited [17,26]. Here, we expand the utility of sybody selection by employing it as a tool
207 to screen for genetic probes targeting the function of selected molecular machines *in vivo*. This strategy
208 combines the advantages of controlled biochemical reconstitution with the ability to study the function
209 of proteins in their native context. Importantly, sybody selection requires no prior knowledge of
210 vulnerable regions, providing an unbiased means to interrogate protein function that is difficult to
211 achieve through rational design. Our study based on the *B. subtilis* Smc-ScpAB DNA motor as a model
212 uncovers a central regulatory region in the coiled coil arms of Smc and highlight how distinct arm
213 conformations shape SMC function in loop extrusion and chromosome segregation.

214

215 **Revealing Smc arm dynamics through synthetic binders**

216 All fourteen Smc-disrupting sybodies share the loop library design. Moreover, their Smc binding sites
217 map to the two short coiled coil segments flanking the conserved 4N arm-to-arm contact, a region that
218 has previously been implicated in key conformational transitions during arm opening [13]. While the
219 fourteen sybodies harbour different epitope binding sequences, we suspect that they may all bind to
220 the Smc dimer in an analogous manner. With the long CDR3 loops known to bind narrow structural
221 cavities[12,27], we speculate that these sybodies may intercalate between the two coiled coil arms (Figure
222 3D). Structural studies are needed to test this hypothesis directly, however, our attempts at X-ray
223 crystallography and electron microscopy of Smc-sybody complexes have failed so far.

224 Notably, while the coiled coil dimer appears similarly structured from the elbow to the hinge [9] (Figure
225 3D), no Smc-disrupting sybodies mapped to regions further away from the 4N contact (Figure 3D). This
226 indicates that opening and closure of the Smc arms might be dispensable at these places, although

227 formal testing would require isolating binders efficiently targeting these regions, potentially facilitated
228 by binder design, and expressing them in *B. subtilis*. This parallels with recent findings with the bacterial
229 SMC defense system Wadjet, where hinge-proximal arm opening is dispensable for loop extrusion, but
230 essential for obstacle bypass [7]. Alternatively, these arm-to-arm contacts might be more stable and thus
231 less likely to be interfered with by sybody binding. Similarly, sybodies targeting below the 4N contact
232 all reduce the ATPase rate (or rather its DNA stimulation), indicating that artificial opening at this
233 position may not disrupt Smc function (Figure S7). Again, these hypotheses need to be tested more
234 directly. We envision that the design of protein binders may allow us to confirm these observations and
235 further dissect the underlying mechanisms.

236 This work establishes sybodies as precision tools for blocking ATP-driven machines inside bacterial cells.
237 By targeting allosteric control points in Smc, they enable mechanistic dissection of loop extrusion and
238 open new avenues for studying dynamic complexes *in vivo*. More broadly, the study demonstrates how
239 synthetic binders can trap or block conformations of active chromatin-associated machines, providing
240 a powerful means to probe their mechanisms in living cells. Looking ahead, the rational design of
241 protein binders with tailored geometry and allosteric potential could allow researchers to manipulate
242 and visualize specific conformational states with even greater control and refinement, across both
243 prokaryotic and eukaryotic organisms, while the generation and *in vivo* screening of sybodies remains
244 an attractive approach to gain unexpected biological insights in an unbiased manner.

245

246 **Material and Methods**

247 ***Bacillus subtilis* strains construction and growth**

248 *B. subtilis* strains used in this study were derived from the parental strain 1A700. Allelic replacement
249 was achieved via double-crossover recombination at the endogenous *smc* locus using the natural
250 competence method described by [18,28]. Chromosome-integration of sybody genes were performed by
251 transforming a vector containing an *amyE h*omologous regions on each side of the recombinant gene
252 of interest, as described in [18]. Transformants were selected on ONA solid medium containing the
253 appropriate antibiotics. Following transformation, strains were purified by single colony isolation and
254 verified through a combination of marker testing, phenotype assessment, PCR, and Sanger sequencing
255 of the *smc* locus, when appropriate. For spot assays, cells were cultured to stationary phase in liquid
256 LB medium, and 9^{-2} and 9^{-5} dilutions were then spotted onto solid ONA medium with chloramphenicol
257 (5 ug/mL) and xylose (0.5% w/v) when induction of the P_{xyl} promoter was required. The strains,
258 plasmids, and oligonucleotides used in this study are listed in Table S4, Table S5 and Table S6,
259 respectively.

260 For viability assessment, 200 LB medium was inoculated with a 1:1000 dilution of a dense *B. subtilis*
261 culture and grown to stationary phase. The culture was then serially diluted in LB medium. From each
262 dilution (9^{-1} to 9^{-8}), 5 µL was spotted onto LB agar plates containing the appropriate antibiotic selection.
263 Plates were incubated, and viability was assessed by imaging the spots at 16- and 24-hours post-
264 incubation.

265 **Sybody selection**

266 Sybody selection was performed following the protocol by [16], with modifications to include binders
267 specific for the ATP/DNA-stabilized "open" form of the *bsuS*mc-ScpAB complex.

268 **Ribosome Display**

269 The standard WTB buffer (50 mM Tris/acetate pH7.4, 150 mM NaCl, 50 mM MgAc2) and its derivatives
270 were adjusted to 50 mM NaCl to facilitate *bsuS*mc-ScpAB binding to dsDNA. The target complex was
271 assembled by mixing 500 nM *bsuS*mc(C119S, C437S, C826S, E1118Q, R643C)-ScpAB, 2 mM ATP, and 5
272 µM 40 bp dsDNA in WTB-D-BSA buffer (WTB including 0.5% (w/v) BSA and 0.1% Tween-20), incubated
273 for 15 min at room temperature (RT). The ribosome display panning solution was supplemented with
274 2 mM ATP and 5 µM dsDNA to maintain binding conditions. Solution panning and biotinylated target
275 capture were conducted at RT to optimize selection for the "open" complex. Washing steps
276 incorporated 2 mM ATP and 5 µm 40 bp dsDNA, while elution, reverse transcription, and cDNA
277 amplification followed the original protocol. Reverse transcribed RNA molecules were quantified by
278 qPCR.

279 **First round of phage display**

280 Phagemid libraries were cloned and electroporated into *E. coli* SS320 as previously described[16]. Phage
281 production was performed using M13KO7 helper phage. The phage display buffer (TBSM) consisted of
282 20 mM Tris-HCl (pH 7.4), 50 mM NaCl, and 2 mM MgCl2. Target preparation involved incubating 500
283 nM biotinylated *bsuS*mc(C119S, C437S, C826S, E1118Q, R643C)ScpAB with 2 mM ATP and 5 µM dsDNA
284 in TBSM-BSA-D (TBSM including 0.5% (w/v) BSA and 0.05% Tween-20). Phages (10^{12}/ml) were incubated
285 with the target at 50 nM for 20 min at RT before immobilization on neutravidin-coated plates. Washing
286 (with added 2 mM ATP and 5 µm 40 bp dsDNA) and elution otherwise followed the original protocol,
287 with enrichment assessed by qPCR. Amplified phages were used for a second selection round.

288 **Second round of phage display**

289 Purified phages from the first round were used at 5×10^{13} phages/ml, and the target was prepared as
290 in the first round. Phage-target binding occurred at 50 nM in the presence of ATP and dsDNA, followed
291 by capture on magnetic beads. A competition step using non-biotinylated *bsuS*mc-ScpAB (1 µM) was
292 included before washes with TBSM-D. Phages were eluted and enrichment was determined by qPCR.
293 Phagemids were purified, sub-cloned into the pNb_init vector, and transformed into *E. coli* MC1061.

294 **Growth curve analyses**

295 Growth curves were generated from *B. subtilis* strains grown overnight to exponential phase in LB
296 medium supplemented with 0.5% glucose, incubated at 30°C with shaking. The following day, fresh 5
297 mL LB cultures were inoculated with the overnight culture to an OD of 0.005 and incubated at 37°C
298 with shaking until reaching an optical density (OD) of 0.05. Subsequently, each culture was subjected
299 to a twofold dilution in a 96-well plate (Costar #3596), achieving a final volume of 200 µL per well.
300 Where necessary, cultures were induced with 0.5% xylose. Plates were incubated at 37°C with
301 continuous shaking in a Thermo Scientific Multiskan FC plate reader. Growth curves were determined
302 by light scattering at 620 nm. The BactEXTRACT app was used to perform Analysis and visualization of
303 the data [29].

304 **Protein purification**

305 **Purification of *bsuS*mc and biotinylated *bsuS*mc(C119S, C437S, C826S, E1118Q, R643C)**

306 *bsuS*mc proteins were purified according to [14]. pET-22 or pET-28 plasmids encoding the *Smc*
307 recombinant sequences were transformed into *E. coli* BL21-Gold (DE3) cells. Protein expression was
308 carried out in ZYM-5052 autoinduction medium for 23 hours at 24°C. The cells were harvested and
309 resuspended in lysis buffer (50 mM Tris-HCl, pH 7.5, 150 mM NaCl, 1 mM EDTA, 1 mM DTT, 10% (w/v)
310 sucrose) supplemented with protease inhibitor cocktail. Cell lysis was achieved by sonication, and the
311 lysate was clarified by centrifugation. The supernatant was filtered through a 0.45 µm membrane and
312 loaded onto two HiTrap Blue HP 5 mL columns connected in series. Elution was performed using lysis
313 buffer with 1 M NaCl. The main peak fractions were pooled and diluted with salt-free buffer (50 mM
314 Tris-HCl, pH 7.5; 1 mM EDTA; 1 mM DTT) to a final conductivity equivalent to 50 mM NaCl (~8 mS/cm).
315 This diluted sample, supplemented with protease inhibitor cocktail, was applied to a HiTrap Heparin
316 HP 5 mL column, and the proteins were eluted using a linear gradient up to 2 M NaCl. The main peak
317 fractions (~ 5 mL) were collected and subjected to further purification by gel filtration using an XK 16/70
318 Superose 6 PG column equilibrated with 50 mM Tris-HCl, pH 7.5, 200 mM NaCl, 1 mM EDTA, and 1 mM

319 TCEP. The peak fractions were collected, concentrated using a Vivaspin 15 10K MWCO filter, flash frozen
320 in liquid nitrogen, and stored at -80°C. Protein concentration was determined by absorbance, utilizing
321 theoretical molar absorption and molecular weight values.

322 For the biotinylated *bsu*Smc(C119S, C437S, C826S, E1118Q, R643C) protein used in the sybody
323 selection, the protein was first purified as described above, except that the reducing agent (TCEP) was
324 omitted from the final gel filtration buffer. Labelling was performed by incubating 600 µL of
325 *bsuS*mc(C119S, C437S, C826S, E1118Q, R643C) (83 µM in 50 mM Tris-HCl pH 7.5, 200 mM NaCl) with 1
326 mM PEG2-biotin maleimide for 10 minutes at 4 °C. The reaction was quenched by addition of 0.5 mM
327 2-mercaptoethanol. Excess label was removed using Zeba spin desalting columns (Thermo Fisher) in
328 multiple parallel runs due to volume limitations. The final yield was 600 µL at 72.35 µM (subunit
329 concentration). Labelled *bsuS*mc(C119S, C437S, C826S, E1118Q, R643C) was loaded onto a Superose 6
330 10/300 Increase column pre-equilibrated in 50 mM Tris-HCl pH 7.5, 200 mM NaCl. Peak fractions were
331 pooled and mixed with ScpA and ScpB at a 1:1:2 molar ratio relative to the *bsuS*mc dimer. The final
332 concentration of the full complex was adjusted to 5.7 µM. Complexes were aliquoted in 100 µL
333 portions, flash-frozen in liquid nitrogen, and stored at −80 °C.

334 **Purification of *bsu*ScpA**

335 ScpA was purified using the method described by[25]. *E. coli* BL21-Gold (DE3) cells, transformed with a
336 pET-28 derived plasmid encoding the ScpA protein, were used for expression. Cultivation was
337 performed in ZYM-5052 autoinduction medium at 16°C for 28 hours. Cells were then harvested and
338 resuspended in lysis buffer (50 mM Tris-HCl, pH 7.5; 200 mM NaCl; 5% glycerol) supplemented with
339 protease inhibitor cocktail. The cells were lysed by sonication, and the lysate was clarified by
340 centrifugation. The supernatant was applied to a 5 mL HiTrap Q ion exchange column and eluted with
341 a gradient up to 2 M NaCl. Peak fractions were pooled and adjusted to a final concentration of 3 M
342 NaCl by mixing with 4 M NaCl buffer. This mixture was loaded onto a HiTrap Butyl HP column and eluted
343 with a reverse gradient to 50 mM NaCl. Eluted peak fractions were concentrated to 5 mL using Vivaspin

344 15 10K MWCO filters and further purified by size exclusion chromatography (SEC) on a HiLoad 16/600
345 Superdex 75 pg column equilibrated with 20 mM Tris-HCl, pH 7.5, and 200 mM NaCl. The purified
346 protein was concentrated, flash frozen, and stored at -80°C.

347 **Purification of *bsu*ScpB**

348 ScpB was purified following the protocol outlined by [25]. The coding sequence of ScpB, cloned into a
349 pET-22 derived plasmid, was transformed into chemically competent BL21-Gold (DE3) *E. coli* cells.
350 These cells were cultivated in ZYM-5052 autoinduction medium at 24°C for 23 hours. Subsequently, the
351 cells were harvested and resuspended in lysis buffer (50 mM Tris-HCl, pH 7.5; 150 mM NaCl; 1 mM
352 EDTA; 1 mM DTT) supplemented with protease inhibitor cocktail. Cell lysis was performed by
353 sonication, followed by centrifugation to remove cell debris. The resulting supernatant was diluted to
354 a final NaCl concentration of 50 mM and loaded onto a 5 mL HiTrap Q HP column. Elution was achieved
355 using a gradient up to 2 M NaCl. The eluate was then diluted with lysis buffer containing 4 M NaCl to
356 achieve a final concentration of 3 M NaCl. This sample was applied to two 5 mL HiTrap Butyl columns
357 connected in series, and the protein was eluted with a reverse gradient to 50 mM NaCl. The peak
358 fractions from this column were concentrated and subjected to size exclusion chromatography (SEC)
359 using a HiLoad 16/600 Superdex 200 pg column equilibrated with 50 mM Tris-HCl, pH 7.5, 100 mM
360 NaCl, and 1 mM DTT. Fractions containing ScpB were concentrated, flash frozen, and stored at -80°C.

361 **Medium scale sybody purification**

362 Individual sybody plasmids were transformed into chemically competent *E. coli* MC1061 cells via heat
363 shock at 42 °C for 45 s, followed by recovery in LB medium at 37 °C. Transformed cells were cultured
364 overnight in TB medium supplemented with 25 µg/ml chloramphenicol. Precultures were used to
365 inoculate 50 mL TB cultures, which were grown at 37 °C before shifting to 22 °C. Expression was induced
366 with 0.02% (wt/vol) L-(+)-arabinose and continued overnight at 22 °C with shaking. Cells were
367 harvested by centrifugation and resuspended in periplasmic extraction buffer. Following incubation at
368 4 °C, cells were pelleted, and the supernatant was supplemented with imidazole to 15 mM. The extract

369 was incubated with His MultiTrap HP resin, followed by centrifugation and washing with TBS containing
370 30 mM imidazole. Elution was performed using TBS with 300 mM imidazole. Purified sybodies were
371 analyzed on a Sepax SRT-10C SEC100 column at 1 ml/min flow rate. Monomeric sybodies eluted
372 between 11–12.5 ml, while retention volumes <11 ml indicated oligomerization, and >14 ml suggested
373 strong column interaction. Non-expressed, oligomeric, or highly interacting sybodies were discarded.
374 Typical yields ranged from 200 µg to 1 mg [16].

375 **Fluorescence imaging of ParB-GFP strains**

376 **Image acquisition**

377 *B. subtilis* cells were first cultured in LB supplemented with 5 µg/mL chloramphenicol and 0.5% glucose
378 at 30°C, from which a day culture was inoculated to 0.005 in LB with 5 µg/mL chloramphenicol. When
379 needed, cultures were induced at OD_{600} ~ 0.02 with 0.5% xylose and grown an extra 30 minutes until
380 imaging at an OD_{600} of 0.04. For microscopy analysis, 0.5 µL of the cell suspension was spotted onto
381 agarose-coated microscopy slides. Images were acquired using a Leica DMi8 microscope equipped with
382 an sCMOS DFC9000 (Leica) camera, a SOLA light engine (Lumencor), and a 100×/1.40 oil-immersion
383 objective. Exposure time for image acquisition was set to 600 ms. Acquired images were processed
384 using LAS X Office software (v.1.4.7.28982, Leica Microsystems).

385 **Image analysis**

386 Microscopy images were analyzed using a fully automated image processing pipeline. Cell
387 segmentation was performed with the pretrained Omnipose model[30] implemented in Cellpose[31], which
388 is optimized for bacterial morphologies. Prior to segmentation, a normalization step was applied to
389 standardize image contrast. Following segmentation, intracellular foci were detected using Spotiflow[32],
390 a dedicated model trained for spot identification. Each detected spot was assigned to an individual cell
391 based on spatial location, enabling quantification of the number of foci per cell. Cell morphology
392 analysis was also performed to estimate cell length.

393 Quantitative results were compiled into a structured dataset, including the number of cells per image,
394 percentage of cells lacking foci, number of foci per cell, cell length, and number of foci per micron. Data
395 visualization and statistical analysis was performed using GraphPad Prism 10.4.1 (627).

396 **ELISA**

397 *E. coli* MC1061 colonies were screened for sybody expression, and periplasmic extracts were obtained
398 as per the original protocol [16]. ELISA plates were coated with Protein A and anti-c-Myc antibody before
399 incubation with sybody-containing extracts. Three wells per sybody were incubated with biotinylated
400 maltose binding protein (MBP, negative control) or with 50 nM biotinylated bsSmc-ScpAB(E1118Q) with
401 ATP/dsDNA or without. Washes and ELISA development were performed using TBSM-D. Absorbance
402 was measured at 650 nm.

403 **ATPase measurements**

404 ATPase activity was assessed using the coupled pyruvate kinase/lactate dehydrogenase reaction as
405 described by [14]. ADP production was monitored over a period of 1 hour by measuring the absorbance
406 changes of NADH at 340 nm. Data collection was performed using a Synergy Neo Hybrid Multi-Mode
407 Microplate Reader. The reaction mixture comprised 1 mM NADH, 3 mM phosphoenolpyruvic acid, 100
408 U pyruvate kinase, 20 U lactate dehydrogenase, and varying concentrations of ATP. For assays requiring
409 double-stranded oligonucleotides, a 40 bp oligonucleotide (5'-TTAGTTGTTC GTAGTGCTCG TCTGGCTCTG
410 GATTACCCGC-3') was added to a final concentration of 3 mM. The final protein concentration in the
411 assay was 0.15 µM *bsuS*mc dimers in ATPase assay buffer (50 mM HEPES-KOH, pH 7.5; 50 mM NaCl; 2
412 mM MgCl2). All measurements were conducted at 25°C.

413 **Acknowledgments**

414 We are grateful to Roberto Vazquez Nunez for the biotinylated *bsuS*mc(C119S, C437S, C826S, E1118Q,
415 R643C) protein preparation, Arianna Ravera from the DCSR computing facility for help in image analysis

and data extraction of the fluorescence microscopy images. Members of the Gruber Lab for critical feedback of the manuscript and for stimulating discussions.

Funding

This study was supported by internal funding and by the European Research Council (Horizon 2020 ERC CoG 724482).

Author contributions

O.G. performed all *in vivo* experiments from sybody selection, fluorescence microscopy imaging, chimeric phenotypic screen. M.T. and L.H-H. performed the *in vitro* sybody screening (ribosome display, phage display, and first sybody purification). O.G. performed protein purifications, cross-linking and ATPase measurements, as well as data analysis, figures and writing. O.G. wrote the first manuscript draft. All authors reviewed and edited the manuscript. Funding acquisition and supervision, S.G.

Competing interests

The authors declare that they have no competing interests.

Data and materials availability

All raw data will be made available at Mendeley Data DOI: 10.17632/k6k62p7z2s.1 (https://data.mendeley.com/datasets/k6k62p7z2s/1).

434 **Figure Legends**

435 **Figure 1: Selection of sybodies targeting *S*mc-ScpAB in *B. subtilis*.**

436 **(A) (i)** Structural design and randomization scheme of the three synthetic sybody libraries: concave,
437 loop, and convex. Complementarity-determining regions (CDRs) 1, 2, and 3 are shown in yellow, orange,
438 and red, respectively; randomized residues are shown as sticks. Adapted from [1]. **(ii)** SMC domain
439 organization. The N- and C-terminal regions encode half an ATPase head, while the middle domain
440 constitutes the hinge dimerization domain. The elongated sequence in-between encodes for long
441 helical sequences that will form an antiparallel intramolecular coiled coil. Hd: head, Hng: hinge, 4N: 4N
442 arm-to-arm contact, J: joint. **(iii)** SMC complexes harbor juxtaposed arms in their resting state. Upon
443 ATP binding at the heads, the heads dimerize (head engagement), leading to a conformational change
444 of the entire complex in which the arms open. This state is thought to fit a loop of DNA (not shown) in
445 the S compartment formed by the SMC arms, that will be pushed towards the K compartment formed
446 by the heads and kleisin, after ADP release. We hypothesized that SMC-blocking sybodies can stabilize
447 distinct conformation of the *bsuS*mc-ScpAB complex promoted by ATP hydrolysis and DNA binding,
448 potentially inducing a *Δsmc*-like phenotype *in vivo* and enabling biochemical characterization of
449 trapped conformations *in vitro*. Blue: SMC dimer, Green: kleisin ScpA. The ScpB KITE subunits are not
450 represented for the sake of simplicity. HngDBS: Hinge DNA-binding site, HdDBS: Head DNA-binding site.

451 **(B)** Framework for sybody selection. *In vitro* selection starts with ~10^{12} sybody variants per library
452 subjected to ribosome display for pre-enrichment, followed by two rounds of phage display. For *in vivo*
453 selection, 95 randomly selected sybody genes were integrated into the *B. subtilis* chromosome under
454 the control of a xylose-inducible promoter by allelic replacement at the *amyE* locus. Growth defects on
455 rich medium were tested on ONA agar plates with or without 0.5% xylose. Example shown: Sb164 (loop
456 library) did not affect growth, whereas Nb31 impaired growth upon induction, suggesting interference
457 with *bsuS*mc function.

458 **(C)** Growth assay results for the 95 *B. subtilis* strains expressing individual xylose-inducible sybodies of
459 the loop library. Bars show colony counts "without" (green) on top of "with" (pink) xylose. Strains are
460 ordered by their original position in the 96-well plate. Fourteen sybodies consistently impaired colony
461 formation under inducing conditions (marked by dotted lines). Sybody numbers indicated above the
462 plots correspond to selected candidates used in subsequent experiments, numbering according to
463 order of first use. Notably, the strain corresponding to the E09 sybody (Sb018), showed an absence of
464 colonies upon sybody induction. However, this sybody candidate gave intermediate phenotypes in later
465 experiments, which is why it was excluded from detailed analysis.

466

467 **Figure 2: Sybody-induced chromosome segregation defects visualized by ParB-GFP imaging.**
468 **(A)** i, *Top*: Schematic illustrating ParB-GFP binding near *oriC*, enabling visualization of origin positioning.
469 *Bottom*: Representative images showing ParB-GFP foci in wild-type and *Δsmc B. subtilis*. *Smc* WT cells
470 typically display 2–4 foci per cell, whereas *Δsmc* cells exhibit reduced foci numbers. ii, Number of ParB-
471 GFP foci per µm of cell length in a strain carrying inducible sybody Sb006. A significant decrease in foci
472 is detected from 40 minutes post-induction (p_{t0-10} = 0.9674; p_{t0-20} = 0.9033; p_{t0-30} = 0.3744; p_{t0-40} =
473 0.0145; p_{t0-50} = 0.0004; p_{t0-60} < 0.001). Based on this, a standardized induction time of ~35 minutes
474 was used in subsequent experiments.

475 **(B)** ParB-GFP foci density (foci/µm) in WT, *Δsmc,* and sybody-expressing strains after 35 minutes of
476 xylose induction. Violin plots show distribution per condition; solid lines denote the mean, and dotted
477 lines indicate quartiles. Several hundreds of cells were analyzed (between 351 and 1735), except for
478 *Δsmc* and Sb010 were fewer cells were available (134 and 73, respectively).

479 **(C)** Spot assay to assess colony formation of *B. subtilis* strains *bsu* or *spn* variants of *S*mc-ScpAB and
480 ParB. *Top*: Schematic shows gene origins (blue: *B. subtilis*; grey: *S. pneumoniae*). The leftmost column
481 corresponds to the parental *B. subtilis* strain 1A700 carrying the *S. pneumoniae* genes without
482 chloramphenicol resistance (non-growing). The next spots represent the same strains carrying no

483 sybody gene but the Cm resistance (EV for empty vector). Remaining spots are sybody-expressing
484 strains; sybody numbers are indicated above. Cells were grown for 16 h at 37 °C on ONA supplemented
485 with 0.5% xylose and chloramphenicol. Hd: head, Hng: hinge, 4N: 4N arm-to-arm contact, J: joint.

486

487 **Figure 3: Mapping sybody binding sites on Smc-ScpAB.**

488 **(A)** Colony formation of *B. subtilis* strains expressing chimeric Smc-ScpAB complexes comprising *S.*
489 *pneumoniae* and *B. subtilis* sequences. The schematic above the spot assay depicts the species origin
490 of the *smc* gene, the *scpAB* operon and *parB* gene (blue: *B. subtilis*; grey: *S. pneumoniae*). "–" indicates
491 no insertion at the *amyE* locus; "EV" refers to the empty vector control containing only the
492 chloramphenicol resistance cassette that was inserted in *amyE*; numbered labels correspond to
493 sybodies. Cells were spotted on rich medium (ONA) supplemented with chloramphenicol and xylose
494 and incubated for 16 h at 37 °C. Hd: head, Hng: hinge, 4N: 4N arm-to-arm contact, J: joint.

495 **(B)** ATP hydrolysis rates of *bsu*Smc-ScpAB in the presence of sybodies but absence of DNA. Significant
496 effects by one-way ANOVA are indicated by p values.

497 **(C)** ATPase rates in the presence of 40 bp dsDNA. All sybodies significantly reduced DNA-stimulated ATP
498 hydrolysis. Reported p-values: Sb020 ($p = 0.340$), Sb194 ($p = 0.0049$), Sb002 ($p = 0.0007$), Sb015 ($p =$
499 0.0003); all others, $p < 0.0001$.

500 **(D)** Schematic summary of sybody binding sites mapped onto the Smc dimer, categorized by their effect
501 on ATPase activity. Sybodies are grouped based on functional impact and mapped to corresponding
502 structural regions: pink/yellow boxes indicate residues 318–339 and 836–857; green boxes mark
503 residues 248–276 and 899–927; and the red box highlights the 4N contact region (approx. residues
504 290–320).

505

506 **Figure 4: Proposed models for sybody interactions with *bsuS*mc-ScpAB during the ATPase cycle.**

Model for sybodies of the Opening^{UP}, Closing^{UP} and Closing^{DOWN} group. Opening^{UP} sybodies, likely prevent complete arm closure. In the presence of DNA, these sybodies may stabilize a suboptimal conformation for head disengagement, resulting in reduced ATPase activity (not shown here). Closing^{UP} and Closing^{DOWN} sybodies stabilize a closed-arm conformation. These likely hinder DNA segments from entering the inter-arm space and accessing the hinge-proximal DNA binding site.

513 **Figure S1: Preparation of *bsuS*mc(C119S, C437S, C826S, E1118Q, R643C)-ScpAB complex and loop**
514 **extrusion model**

515 **(A)** Size-exclusion chromatography profile of biotinylated *bsuS*mc(C119S, C437S, C826S, E1118Q,
516 R643C)-ScpAB complex. Peak fractions (elution at ~13 mL, pooled fractions indicated by dotted lines
517 for a final volume of 1.8 mL) were collected for downstream use; the final concentration was 5.9 µM
518 (dimer). * : A secondary peak appeared at ~14 mL; its identity was uncertain and was excluded from
519 the peak. SDS-PAGE confirms successful biotinylation of the *bsu*Smc(C119S, C437S, C826S, E1118Q,
520 R643C)-ScpAB complex.

521 **(B)** Segment-capture model for *bsuS*mc-ScpAB, in which ATP binding and hydrolysis drive transitions
522 between open and closed conformations to mediate loop extrusion.

523

524 **Figure S2: Representative results from *in vivo* sybody selection based on colony formation.**

525 **(A)** Representative examples of *in vivo* transformation assays for nine sybody-expressing *B. subtilis*
526 strains. Sybody genes were integrated into the *amyE* locus under xylose-inducible control.
527 Transformants were grown on oxoid nutrient agar (ONA) plates supplemented with chloramphenicol
528 and 0.5% xylose to assess growth defects. Shown are candidates from the concave library: Sb051 (well
529 B08) and Sb078 (D12). Loop library: Sb007 (E05), Sb020 (E12), Sb031 (F05), Sb164 (D12) and NbH07
530 (Sb194). Convex library: Sb239 (D12) and Sb248 (E10).

531 **(B)** Growth assay results for the 285 *B. subtilis* strains expressing individual xylose-inducible sybodies.
532 Bars show each colony counts “without” (green) on top of “with” (pink) xylose. Strains are ordered by
533 their original 96-well plate. Only the loop library yielded sybodies that consistently impaired growth
534 under inducing conditions (dotted line). Sybody numbers indicated above the plots correspond to
535 positive candidates used in subsequent experiments, numbered according to order of use. Notably, the
536 strain corresponding to the E09 M sybody (Sb018), also showed an absence of growth upon sybody

537 induction. However, this sybody candidate gave intermediate phenotypes in later experiments, which
538 is why it was excluded from this study. Results for the loop library are also shown in Figure 1.

539

540 **Figure S3: Functional impact of sybody expression on chromosome organization, cell length, and**
541 **growth in *B. subtilis*.**

542 **(A)** Average number of ParB-GFP foci per µm of cell length in strains expressing individual sybodies,
543 with and without xylose induction. Most uninduced strains differed significantly from the Smc WT
544 control, likely due to leaky expression from the P_{xyl} ($p < 0.0001$), except Sb015 ($p > 0.9999$), Sb156
545 ($p = 0.2345$), and Sb016 (negative control, $p > 0.9999$).

546 **(B)** Average cell length across the same conditions, measured in ParB-GFP strains with or without Smc,
547 and with or without each sybody. Bars indicate standard deviation. Tested sybodies caused cell
548 elongation, a characteristic phenotype of impaired Smc activity, as chromosome segregation defects
549 delay cell division, with mean lengths from 4.70 ± 2.16 µm (Sb020) to 8.68 ± 2.99 µm (Sb010), compared
550 to 4.51 ± 1.95 µm in wild-type and 9.96 ± 8.92 µm in Δ*smc*. **(C)** Growth curves of *B. subtilis* strains
551 expressing individual sybodies compared to the WT strain, with and without xylose induction. Each
552 curve represents the mean of two biological replicates. Six sybodies were randomly picked and showed
553 in this figure. Fluorophore-free strains showed wild type-like growth without xylose but strong delays
554 post-induction, followed by partial growth recovery after 12 hours, likely due to xylose depletion or
555 suppressor emergence. In sybody-expressing strains, a clear drop in cell density was observed ~2.5
556 hours post-induction.

557

558 **Figure S4: Sybody-GFP expression at different inducer concentration**

559 Selected Sybody-GFP proteins were tested by GFP imaging at different inducer concentrations (0, 0.005,
560 0.05 and 0.5 % xylose). Representative images are shown. Notably, sybody Sb007 (E5, loop library)

561 generates a mild growth phenotype (smaller colonies but normal colony numbers, Figure 1A and 1B)
562 but shows good expression levels and focal localization (top row).

563

564 **Figure S5: Imaging of various Sybody-GFP proteins without inducer.**

565 Selected Sybody-GFP constructs were grown in the absence of inducer and tested for gfp expression.
566 Representative images are shown.

567

568 **Figure S6: ATPase hydrolysis rate of the *bsuS*mc-ScpAB complex with each selected sybody and**
569 **viability of *B. subtilis* strains expressing chimeric Smc-ScpAB complexes in the absence of sybody**
570 **induction.**

571 **(A)** Spotting assay assessing the growth of *B. subtilis* strains carrying chimeric Smc-ScpAB operons
572 composed of *S. pneumoniae* and *B. subtilis* components. Strains harbor individual sybody constructs
573 integrated at the *amyE* locus under control of a xylose-inducible promoter but were grown without
574 inducer. "–" indicates no integration at *amyE*; "EV" corresponds to an empty vector control containing
575 only the chloramphenicol resistance cassette. Numbered labels indicate strains carrying specific sybody
576 constructs. Cells were spotted on rich medium (ONA) containing chloramphenicol and incubated for
577 16 h at 37 °C.

578 **(B)** Overall ATPase hydrolysis rate of the *bsuS*mc-ScpAB complex in presence of each sybody and +/-
579 DNA. Sb06, 021 and 194 triggered a significant difference in ATP hydrolysis between +/- dsDNA
580 conditions. The rest is non-significant.

581

582 **Figure S7: Hypothetical model for an Opening^{DOWN} class of sybodies, not recovered in this study.**

583 This may indicate that stabilizing an open conformation near the ATPase heads does not interfere with

584 Smc function.

585

586 **Tables**

587 **Table 1: Sybody enrichments at different steps of the selection procedure.**

588 Ribosome display output was quantified by qPCR, while phage display results include final phage titers

589 and enrichment values from rounds one and two, also measured by qPCR.

590 **Table S1: ELISA sybody binding assay**

591 **Table S2: Sybody sequences**

592 **Table S3: Percentage of cells lacking ParB-GFP foci**, indicating the absence of chromosome due to

593 segregation defect. In presence and absence of xylose for sybody induction.

594 **Table S4: Strains**

595 **Table S5: Plasmids**

596 **Table S6: Oligonucleotides**

597

598 **References**

599 1. Zimmermann, I., Egloff, P., Hutter, C.A., Arnold, F.M., Stohler, P., Bocquet, N., Hug, M.N., Huber,
600 S., Siegrist, M., Hetemann, L., et al. (2018). Synthetic single domain antibodies for the
601 conformational trapping of membrane proteins. Elife *7*. 10.7554/eLife.34317.
602 2. Pacesa, M., Nickel, L., Schellhaas, C., Schmidt, J., Pyatova, E., Kissling, L., Barendse, P.,
603 Choudhury, J., Kapoor, S., Alcaraz-Serna, A., et al. (2025). One-shot design of functional protein
604 binders with BindCraft. Nature *646*, 483-492. 10.1038/s41586-025-09429-6.
605 3. Yatskevich, S., Rhodes, J., and Nasmyth, K. (2019). Organization of Chromosomal DNA by SMC
606 Complexes. Annu Rev Genet *53*, 445-482. 10.1146/annurev-genet-112618-043633.
607 4. Burmann, F., and Gruber, S. (2015). SMC condensin: promoting cohesion of replicon arms. Nat
608 Struct Mol Biol *22*, 653-655. 10.1038/nsmb.3082.
609 5. Gruber, S., and Errington, J. (2009). Recruitment of condensin to replication origin regions by
610 ParB/SpoOJ promotes chromosome segregation in B. subtilis. Cell *137*, 685-696.
611 10.1016/j.cell.2009.02.035.
612 6. Wang, X., Tang, O.W., Riley, E.P., and Rudner, D.Z. (2014). The SMC condensin complex is
613 required for origin segregation in Bacillus subtilis. Curr Biol *24*, 287-292.
614 10.1016/j.cub.2013.11.050.
615 7. Liu, H.W., Roisne-Hamelin, F., Taschner, M., Collier, J., Srinivasan, M., and Gruber, S. (2025). The
616 SMC Hinge is a Selective Gate for Obstacle Bypass. Nat Commun *16*, 10457. 10.1038/s41467-
617 025-65408-5.
618 8. Sullivan, N.L., Marquis, K.A., and Rudner, D.Z. (2009). Recruitment of SMC by ParB-parS
619 organizes the origin region and promotes efficient chromosome segregation. Cell *137*, 697-707.
620 10.1016/j.cell.2009.04.044.
621 9. Diebold-Durand, M.L., Lee, H., Ruiz Avila, L.B., Noh, H., Shin, H.C., Im, H., Bock, F.P., Burmann,
622 F., Durand, A., Basfeld, A., et al. (2017). Structure of Full-Length SMC and Rearrangements
623 Required for Chromosome Organization. Mol Cell *67*, 334-347 e335.
624 10.1016/j.molcel.2017.06.010.
625 10. Marko, J.F., De Los Rios, P., Barducci, A., and Gruber, S. (2019). DNA-segment-capture model
626 for loop extrusion by structural maintenance of chromosome (SMC) protein complexes. Nucleic
627 Acids Res *47*, 6956-6972. 10.1093/nar/gkz497.
628 11. Minnen, A., Burmann, F., Wilhelm, L., Anchimiuk, A., Diebold-Durand, M.L., and Gruber, S.
629 (2016). Control of Smc Coiled Coil Architecture by the ATPase Heads Facilitates Targeting to
630 Chromosomal ParB/parS and Release onto Flanking DNA. Cell Rep *14*, 2003-2016.
631 10.1016/j.celrep.2016.01.066.
632 12. Rasmussen, S.G., Choi, H.J., Fung, J.J., Pardon, E., Casarosa, P., Chae, P.S., Devree, B.T.,
633 Rosenbaum, D.M., Thian, F.S., Kobilka, T.S., et al. (2011). Structure of a nanobody-stabilized
634 active state of the beta(2) adrenoceptor. Nature *469*, 175-180. 10.1038/nature09648.
635 13. Vazquez Nunez, R., Polyhach, Y., Soh, Y.M., Jeschke, G., and Gruber, S. (2021). Gradual opening
636 of Smc arms in prokaryotic condensin. Cell Rep *35*, 109051. 10.1016/j.celrep.2021.109051.
637 14. Burmann, F., Basfeld, A., Vazquez Nunez, R., Diebold-Durand, M.L., Wilhelm, L., and Gruber, S.
638 (2017). Tuned SMC Arms Drive Chromosomal Loading of Prokaryotic Condensin. Mol Cell *65*,
639 861-872 e869. 10.1016/j.molcel.2017.01.026.
640 15. Hirano, M., and Hirano, T. (2004). Positive and negative regulation of SMC-DNA interactions by
641 ATP and accessory proteins. EMBO J *23*, 2664-2673. 10.1038/sj.emboj.7600264.
642 16. Zimmermann, I., Egloff, P., Hutter, C.A.J., Kuhn, B.T., Brauer, P., Newstead, S., Dawson, R.J.P.,
643 Geertsma, E.R., and Seeger, M.A. (2020). Generation of synthetic nanobodies against delicate
644 proteins. Nat Protoc *15*, 1707-1741. 10.1038/s41596-020-0304-x.
645 17. Deneka, D., Rutz, S., Hutter, C.A.J., Seeger, M.A., Sawicka, M., and Dutzler, R. (2021). Allosteric
646 modulation of LRRC8 channels by targeting their cytoplasmic domains. Nat Commun *12*, 5435.
647 10.1038/s41467-021-25742-w.

18. Diebold-Durand, M.L., Burmann, F., and Gruber, S. (2019). High-Throughput Allelic Replacement Screening in Bacillus subtilis. Methods Mol Biol *2004*, 49-61. 10.1007/978-1-4939-9520-2_5.
19. Hutter, C.A.J., Timachi, M.H., Hurlimann, L.M., Zimmermann, I., Egloff, P., Goddeke, H., Kucher, S., Stefanic, S., Karttunen, M., Schafer, L.V., et al. (2019). The extracellular gate shapes the energy profile of an ABC exporter. Nat Commun *10*, 2260. 10.1038/s41467-019-09892-6.
20. Gruber, S., Veening, J.W., Bach, J., Blettinger, M., Bramkamp, M., and Errington, J. (2014). Interlinked sister chromosomes arise in the absence of condensin during fast replication in B. subtilis. Curr Biol *24*, 293-298. 10.1016/j.cub.2013.12.049.
21. Bock, F.P., Liu, H.W., Anchimiuk, A., Diebold-Durand, M.L., and Gruber, S. (2022). A joint-ParB interface promotes Smc DNA recruitment. Cell Rep *40*, 111273. 10.1016/j.celrep.2022.111273.
22. Gabler, F., Nam, S.Z., Till, S., Mirdita, M., Steinegger, M., Soding, J., Lupas, A.N., and Alva, V. (2020). Protein Sequence Analysis Using the MPI Bioinformatics Toolkit. Curr Protoc Bioinformatics *72*, e108. 10.1002/cpbi.108.
23. Jumper, J., Evans, R., Pritzel, A., Green, T., Figurnov, M., Ronneberger, O., Tunyasuvunakool, K., Bates, R., Zidek, A., Potapenko, A., et al. (2021). Highly accurate protein structure prediction with AlphaFold. Nature *596*, 583-589. 10.1038/s41586-021-03819-2.
24. Soh, Y.M., Burmann, F., Shin, H.C., Oda, T., Jin, K.S., Toseland, C.P., Kim, C., Lee, H., Kim, S.J., Kong, M.S., et al. (2015). Molecular basis for SMC rod formation and its dissolution upon DNA binding. Mol Cell *57*, 290-303. 10.1016/j.molcel.2014.11.023.
25. Vazquez Nunez, R., Ruiz Avila, L.B., and Gruber, S. (2019). Transient DNA Occupancy of the SMC Interarm Space in Prokaryotic Condensin. Mol Cell *75*, 209-223 e206. 10.1016/j.molcel.2019.05.001.
26. Seeger, M.A., Mittal, A., Velamakanni, S., Hohl, M., Schauer, S., Salaa, I., Grutter, M.G., and van Veen, H.W. (2012). Tuning the drug efflux activity of an ABC transporter in vivo by in vitro selected DARPin binders. PLoS One *7*, e37845. 10.1371/journal.pone.0037845.
27. Kruse, A.C., Ring, A.M., Manglik, A., Hu, J., Hu, K., Eitel, K., Hubner, H., Pardon, E., Valant, C., Sexton, P.M., et al. (2013). Activation and allosteric modulation of a muscarinic acetylcholine receptor. Nature *504*, 101-106. 10.1038/nature12735.
28. Burmann, F., Shin, H.C., Basquin, J., Soh, Y.M., Gimenez-Oya, V., Kim, Y.G., Oh, B.H., and Gruber, S. (2013). An asymmetric SMC-kleisin bridge in prokaryotic condensin. Nat Struct Mol Biol *20*, 371-379. 10.1038/nsmb.2488.
29. Denereaz, J., and Veening, J.W. (2024). BactEXTRACT: an R Shiny app to quickly extract, plot and analyse bacterial growth and gene expression data. Access Microbiol *6*. 10.1099/acmi.0.000742.v3.
30. Cutler, K.J., Stringer, C., Lo, T.W., Rappez, L., Stroustrup, N., Brook Peterson, S., Wiggins, P.A., and Mougous, J.D. (2022). Omnipose: a high-precision morphology-independent solution for bacterial cell segmentation. Nat Methods *19*, 1438-1448. 10.1038/s41592-022-01639-4.
31. Stringer, C., Wang, T., Michaelos, M., and Pachitariu, M. (2021). Cellpose: a generalist algorithm for cellular segmentation. Nat Methods *18*, 100-106. 10.1038/s41592-020-01018-x.
32. Dominguez Mantes, A., Herrera, A., Khven, I., Schlaeppi, A., Kyriacou, E., Tsissios, G., Skoufa, E., Santangeli, L., Buglakova, E., Durmus, E.B., et al. (2025). Spotiflow: accurate and efficient spot detection for fluorescence microscopy with deep stereographic flow regression. Nat Methods *22*, 1495-1504. 10.1038/s41592-025-02662-x.

	Ribosome Display (qPCR)	Phage Display (qPCR)		
Library	**Total #of RNAs**	**Titer (PFU/mL)**	**Enrichment 1**	**Enrichment 2**
Convex (S)	1.36×10^{8}	8.96×10^{13}	3.1×	1474.7×
Loop (M)	6.95×10^{7}	5.46×10^{13}	1.4×	1209.9×
Concave (L)	1.25×10^{8}	8.32×10^{13}	1.8×	1808.0×

Table 1

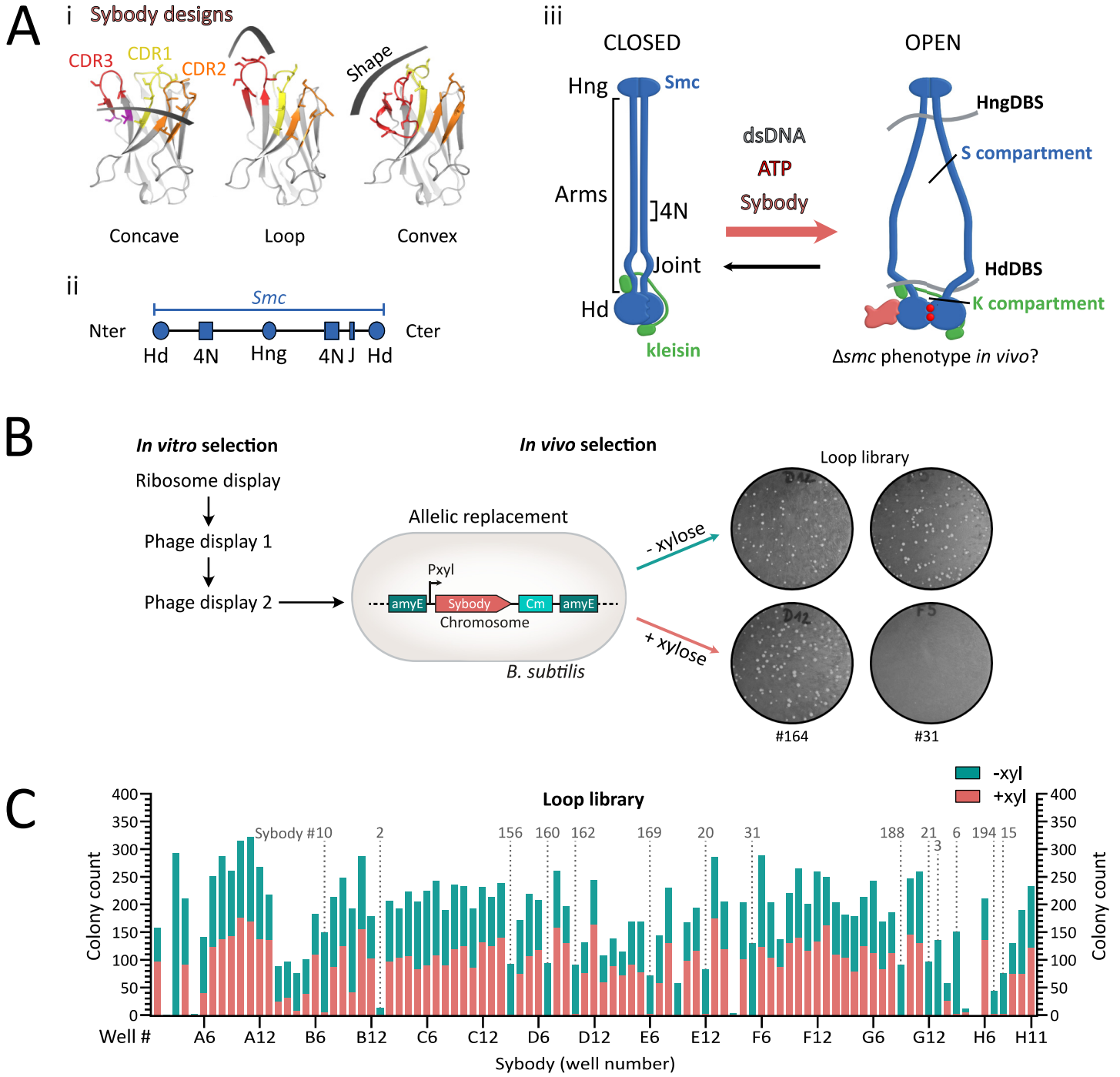
A
i Sybody designs
CDR3
CDR1
CDR2
Shape
Concave
Loop
Convex
ii
Smc
Nter
Cter
Hd
4N
Hng
4N
J
Hd
iii
CLOSED
OPEN
Hng
Smc
Arms
4N
Joint
Hd
kleisin
dsDNA
ATP
Sybody
HngDBS
S compartment
HdDBS
K compartment
Δsmc phenotype in vivo?
B
In vitro selection
Ribosome display
Phage display 1
Phage display 2
In vivo selection
Allelic replacement
Pxyl
amyE
Sybody
Cm
amyE
Chromosome
B. subtilis
- xylose
+ xylose
Loop library
#164
#31
C
Loop library
-xyl
+xyl
Colony count
Sybody #10
2
156
160
162
169
20
31
188
21
3
6
194
15
Well #
A6
A12
B6
B12
C6
C12
D6
D12
E6
E12
F6
F12
G6
G12
H6
H11
Sybody (well number)

Figure 1

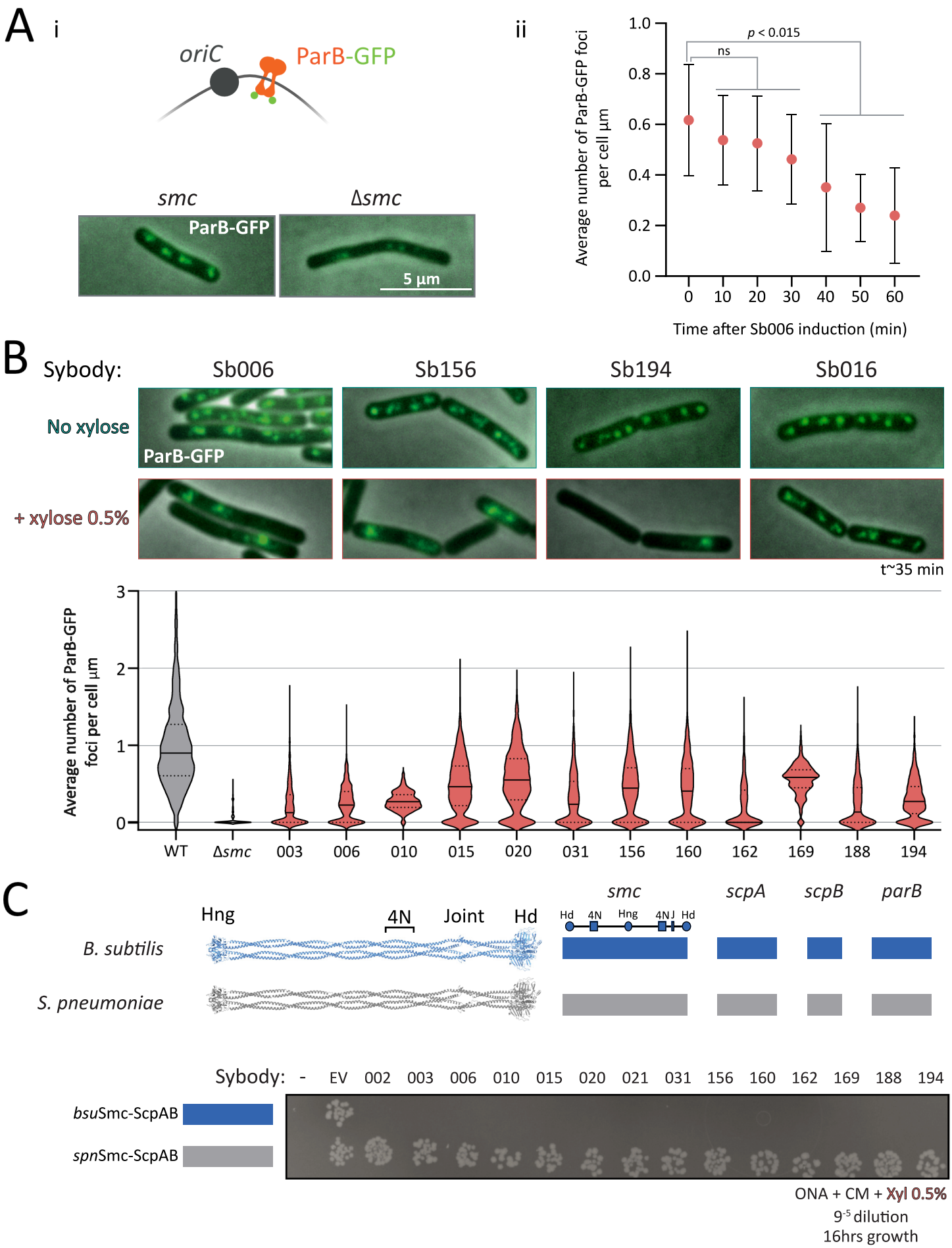
A
i
oriC
ParB-GFP
smc
Δsmc
ParB-GFP
5 µm
ii
Average number of ParB-GFP foci per cell µm
1.0
0.8
0.6
0.4
0.2
0.0
p < 0.015
ns
0
10
20
30
40
50
60
Time after Sb006 induction (min)
B
Sybody:
Sb006
Sb156
Sb194
Sb016
No xylose
ParB-GFP
+ xylose 0.5%
t~35 min
Average number of ParB-GFP foci per cell µm
3
2
1
0
WT
Δsmc
003
006
010
015
020
031
156
160
162
169
188
194
C
Hng
4N
Joint
Hd
B. subtilis
S. pneumoniae
smc
scpA
scpB
parB
Hd
4N
Hng
4N
J
Hd
Sybody:
-
EV
002
003
006
010
015
020
021
031
156
160
162
169
188
194
bsuSmc-ScpAB
spnSmc-ScpAB
ONA + CM + Xyl 0.5%
9-5 dilution
16hrs growth

Figure 2

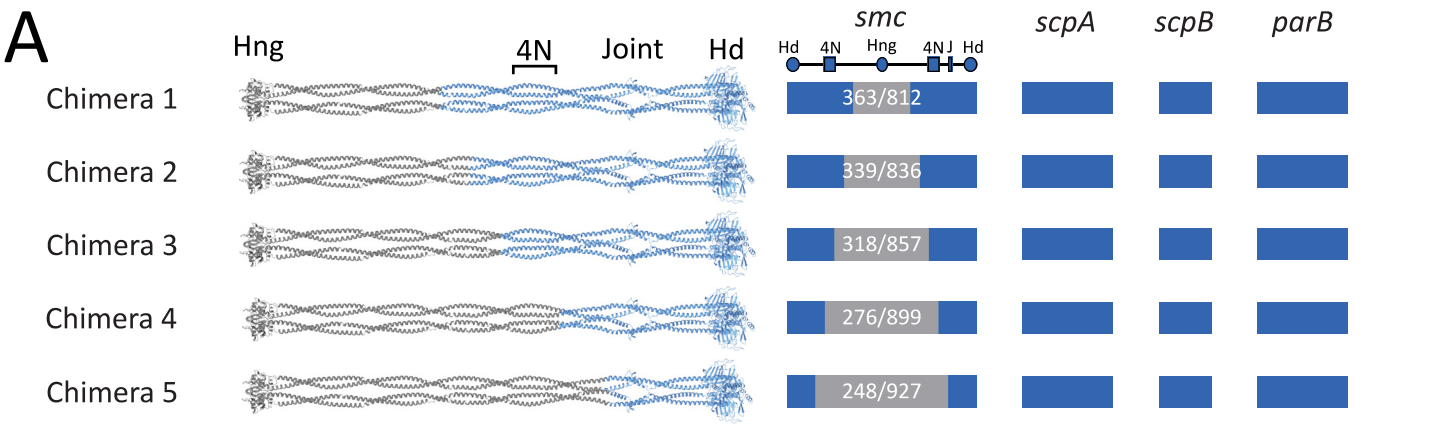
A
Hng
4N
Joint
Hd
smc
Hd 4N Hng 4N J Hd
scpA
scpB
parB
Chimera 1
Chimera 2
Chimera 3
Chimera 4
Chimera 5
363/812
339/836
318/857
276/899
248/927

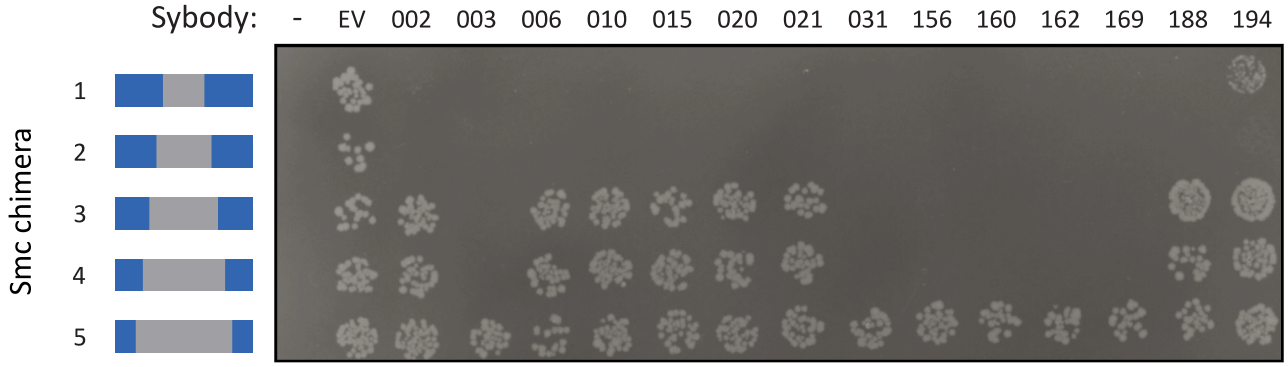
Sybody: - EV 002 003 006 010 015 020 021 031 156 160 162 169 188 194
Smc chimera
1
2
3
4
5

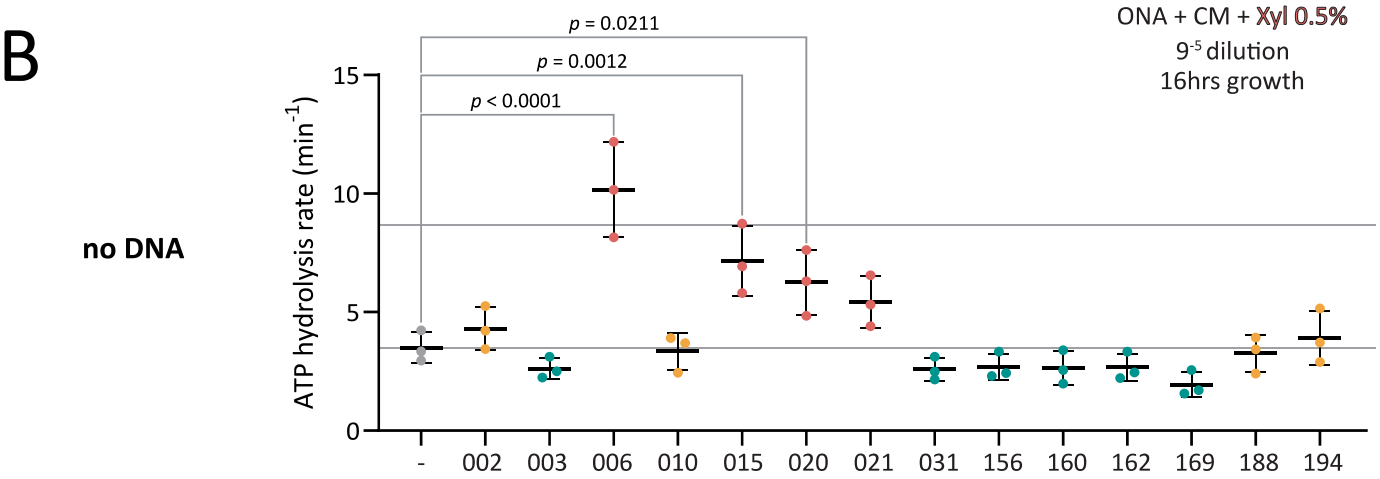
B
ONA + CM + Xyl 0.5%
9-5 dilution
16hrs growth
p = 0.0211
p = 0.0012
p < 0.0001
no DNA
ATP hydrolysis rate (min-1)
15
10
5
0
- 002 003 006 010 015 020 021 031 156 160 162 169 188 194

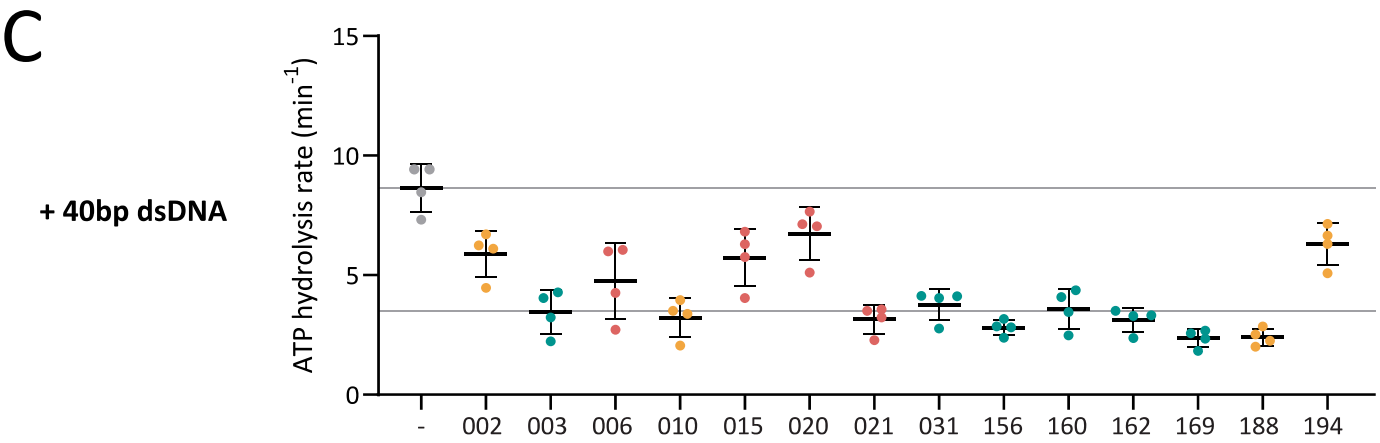
C
+ 40bp dsDNA
ATP hydrolysis rate (min-1)
15
10
5
0
- 002 003 006 010 015 020 021 031 156 160 162 169 188 194

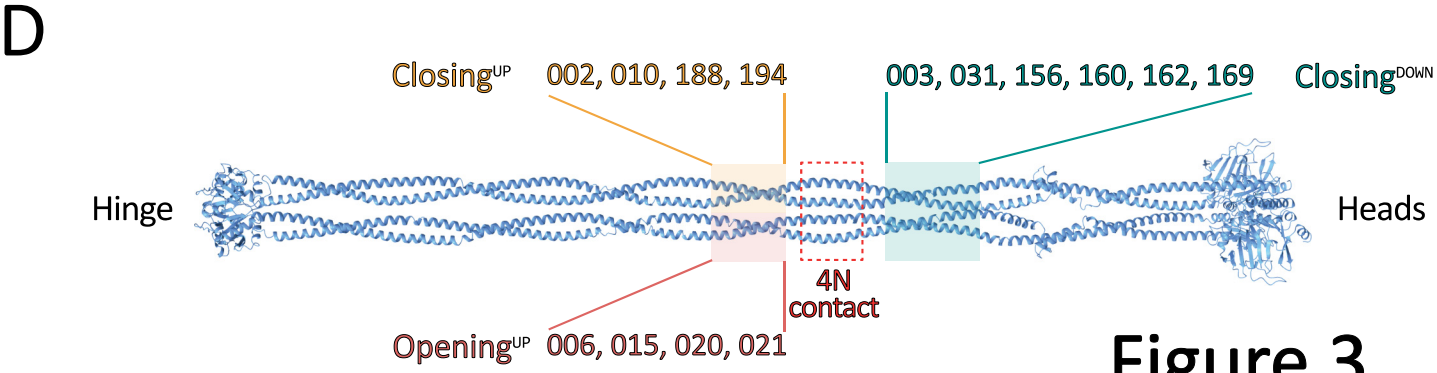
D
ClosingUP 002, 010, 188, 194
003, 031, 156, 160, 162, 169 ClosingDOWN
Hinge
Heads
4N contact
OpeningUP 006, 015, 020, 021

Figure 3

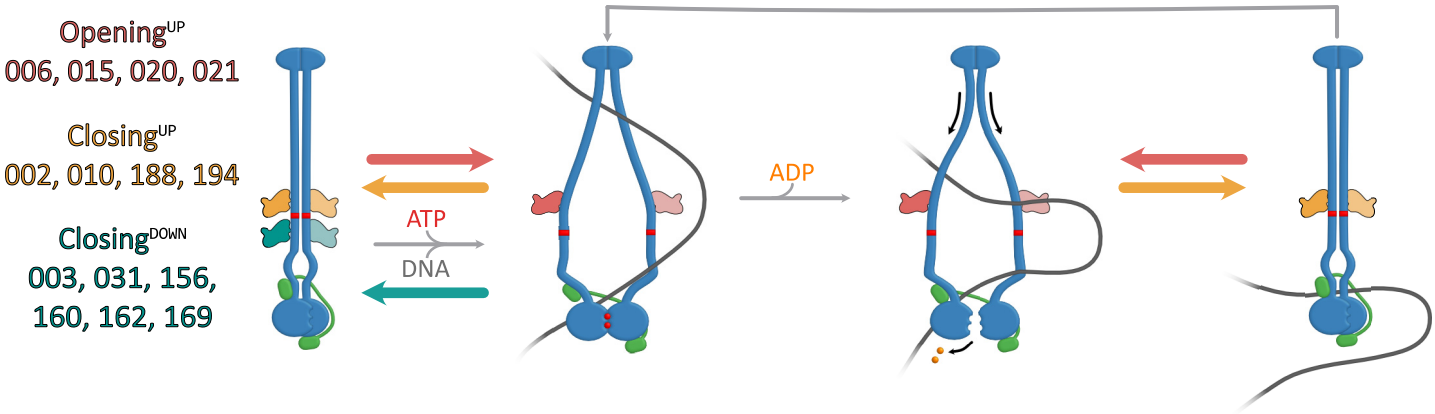
Opening^UP
006, 015, 020, 021
Closing^UP
002, 010, 188, 194
Closing^DOWN
003, 031, 156,
160, 162, 169
ATP
DNA
ADP

Figure 4

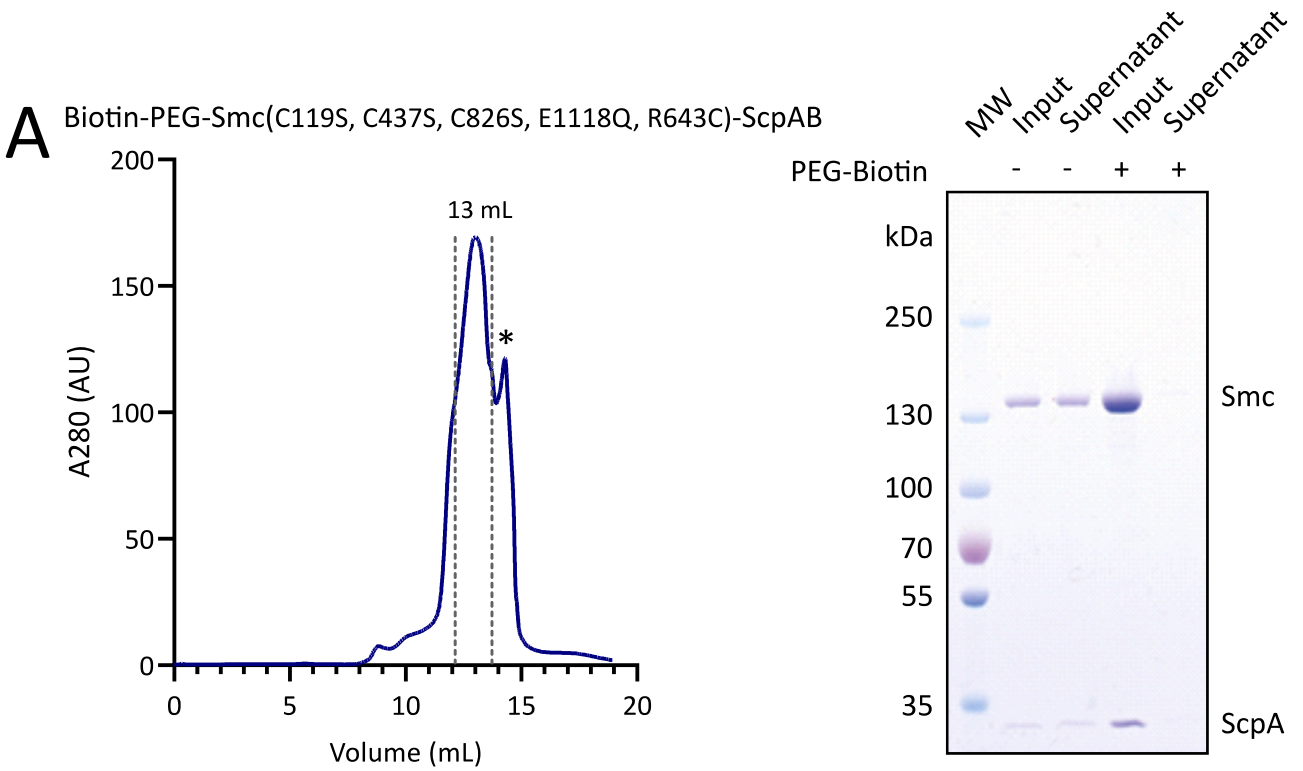
A
Biotin-PEG-Smc(C119S, C437S, C826S, E1118Q, R643C)-ScpAB
13 mL
*
A280 (AU)
Volume (mL)
MW
Input
Supernatant
Input
Supernatant
PEG-Biotin
- - + +
kDa
250
130
100
70
55
35
Smc
ScpA

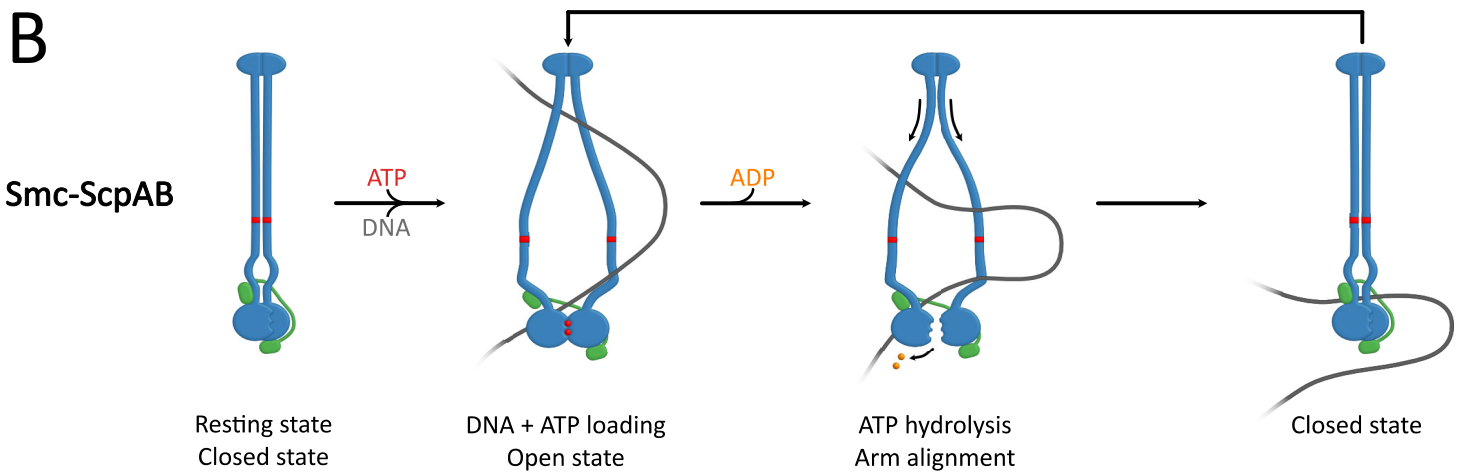
B
Smc-ScpAB
ATP
DNA
ADP
Resting state
Closed state
DNA + ATP loading
Open state
ATP hydrolysis
Arm alignment
Closed state

Figure S1

Figure S2

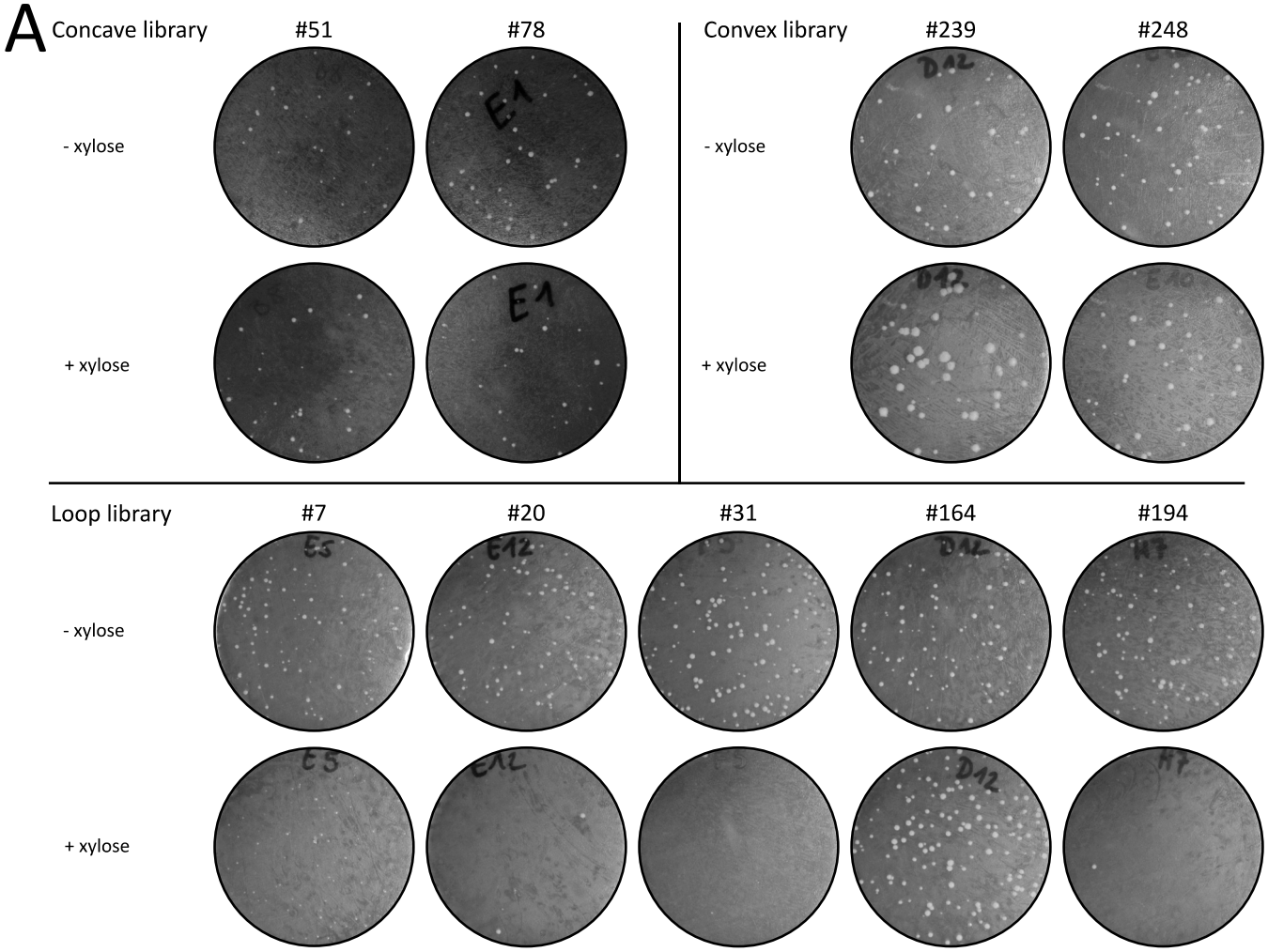
A
Concave library
#51
#78
- xylose
+ xylose
Convex library
#239
#248
- xylose
+ xylose
Loop library
#7
#20
#31
#164
#194
- xylose
+ xylose

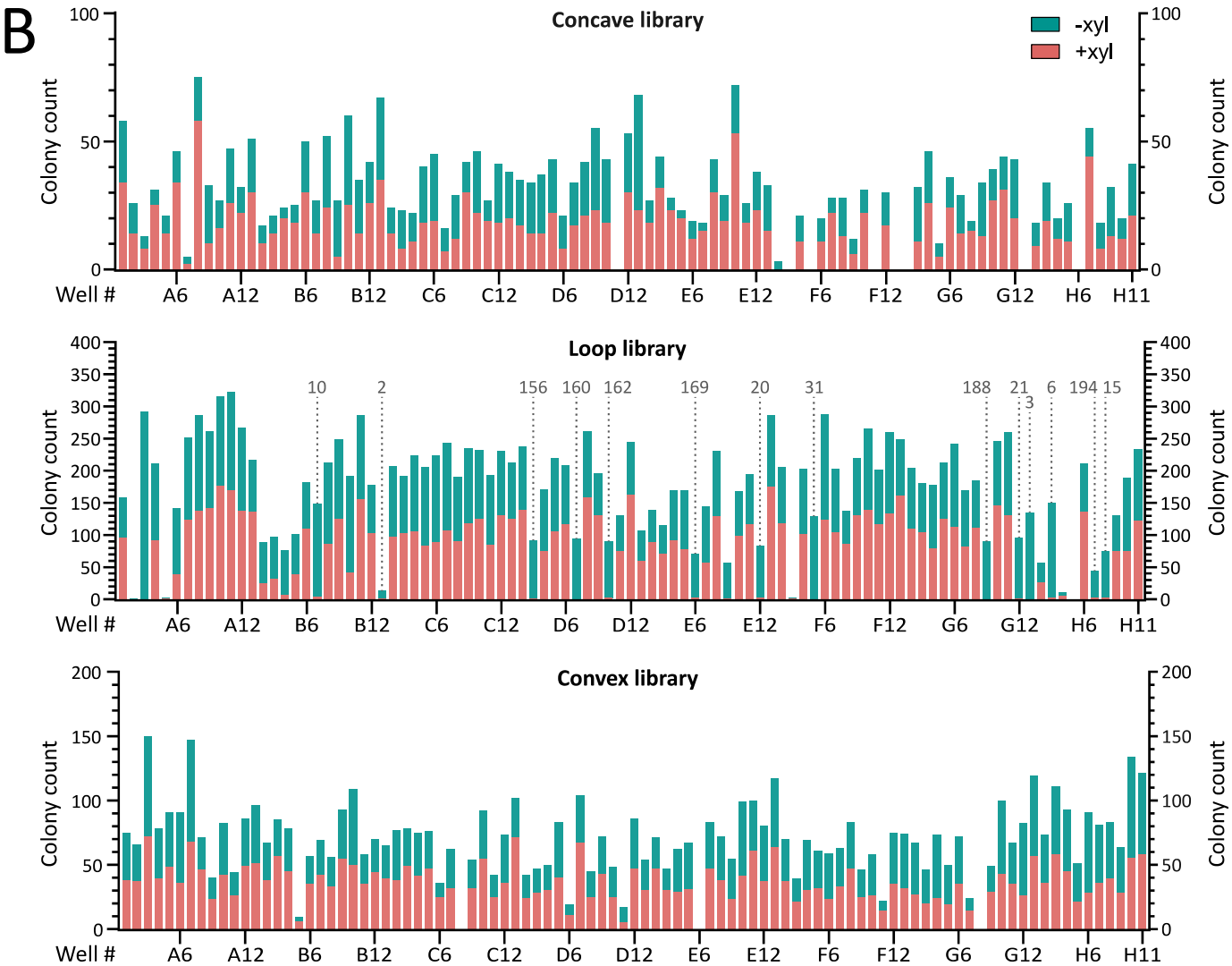
B
Concave library
-xyl
+xyl
Colony count
Well #
A6
A12
B6
B12
C6
C12
D6
D12
E6
E12
F6
F12
G6
G12
H6
H11
Loop library
10
2
156
160
162
169
20
31
188
21
3
6
194
15
Convex library

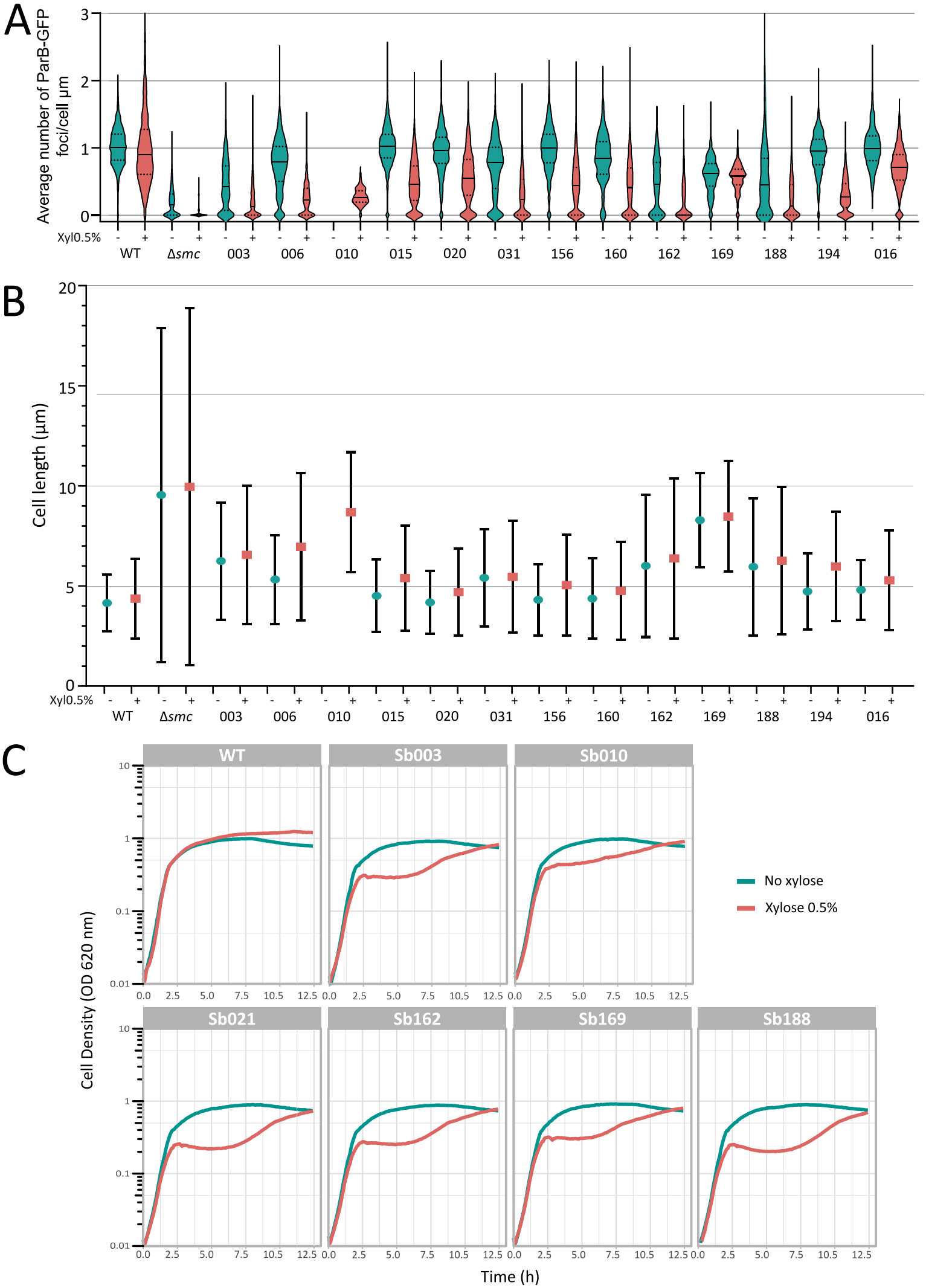
A
Average number of ParB-GFP foci/cell µm
Xyl0.5%
WT
Δsmc
003
006
010
015
020
031
156
160
162
169
188
194
016
B
Cell length (µm)
C
WT
Sb003
Sb010
Sb021
Sb162
Sb169
Sb188
Cell Density (OD 620 nm)
No xylose
Xylose 0.5%
Time (h)

Figure S3

Figure S4: ΔamyE::Sybody-mGFP::CamR::amyE (xylose titration)

No xylose	0.5 % xylose	0.05 % xylose	0.005 % xylose
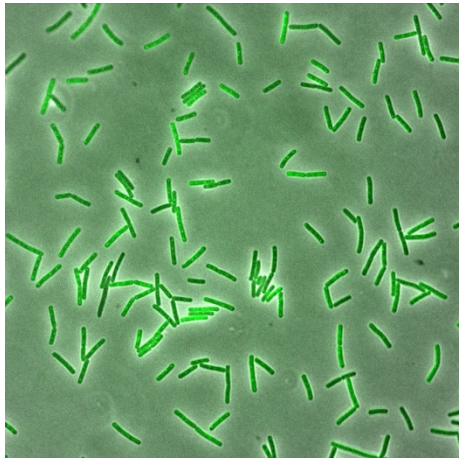	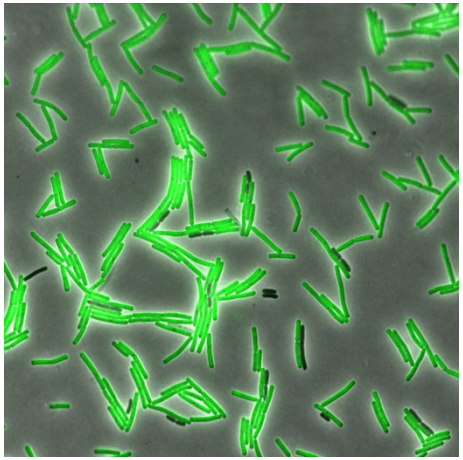	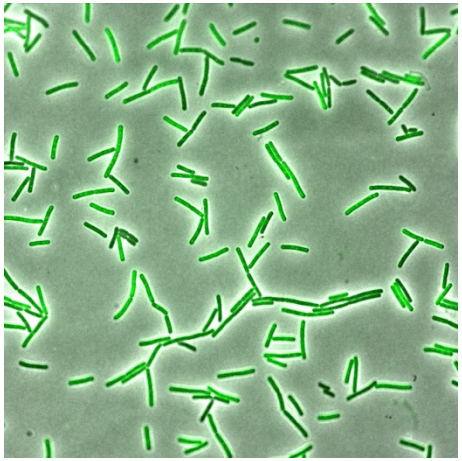	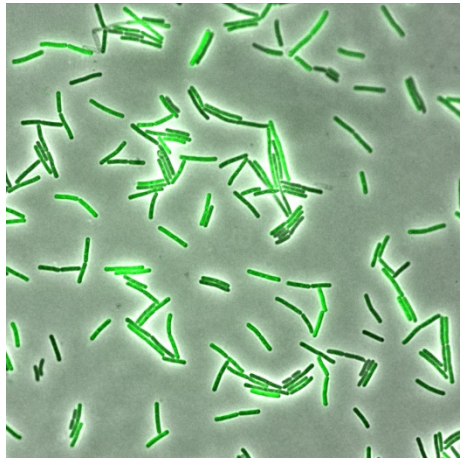
20210825 BSG1001 Sb007 No Xyl 1 001	20210825 BSG1001 Sb007 Xyl 2 002	20210825 BSG1001 Sb007 Xyl 3 002	20210825 BSG1001 Sb007 Xyl 4 003
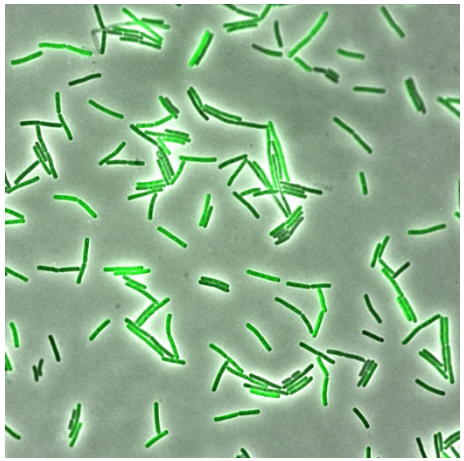	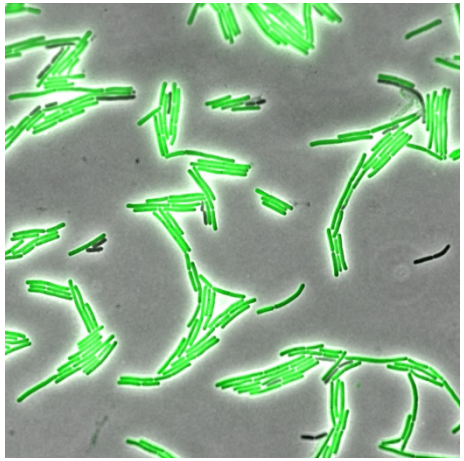	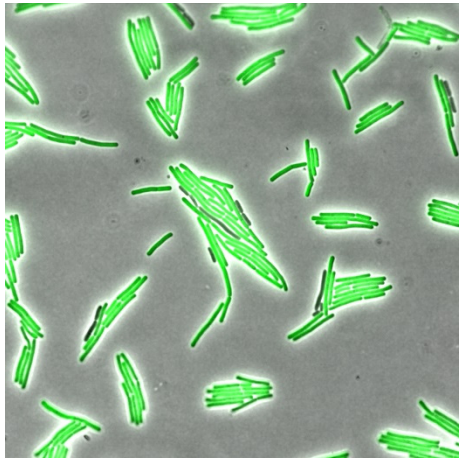	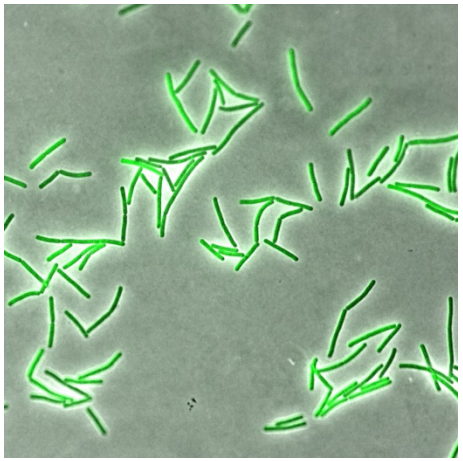
20210825 BSG1001 Sb015 No Xyl 1 002	20210825 BSG1001 Sb015 Xyl 2 002	20210825 BSG1001 Sb015 Xyl 3 001	20210825 BSG1001 Sb015 Xyl 4 005

Figure S5: ΔamyE::Sybody-mGFP::CamR::amyE (No induction)

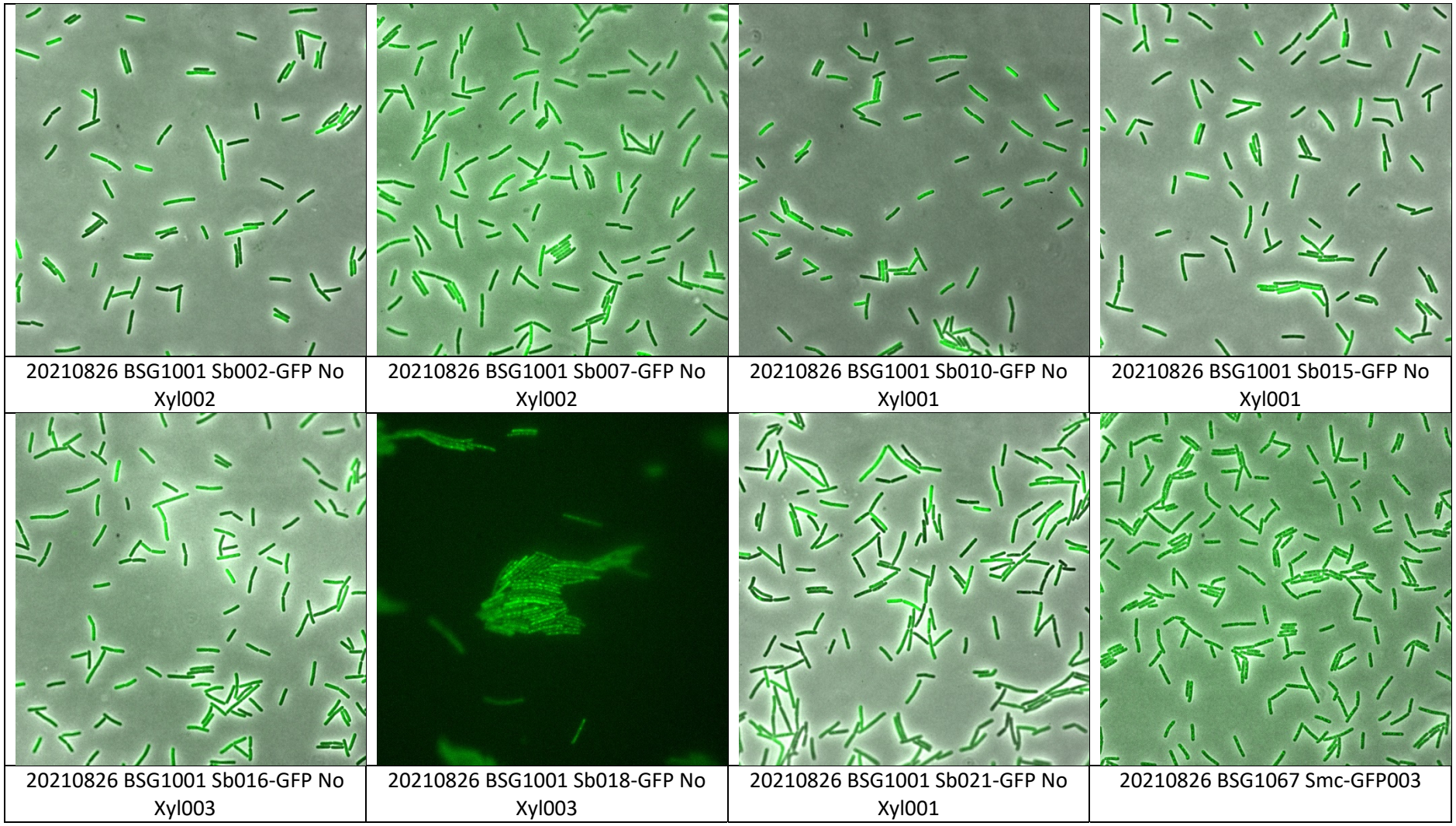

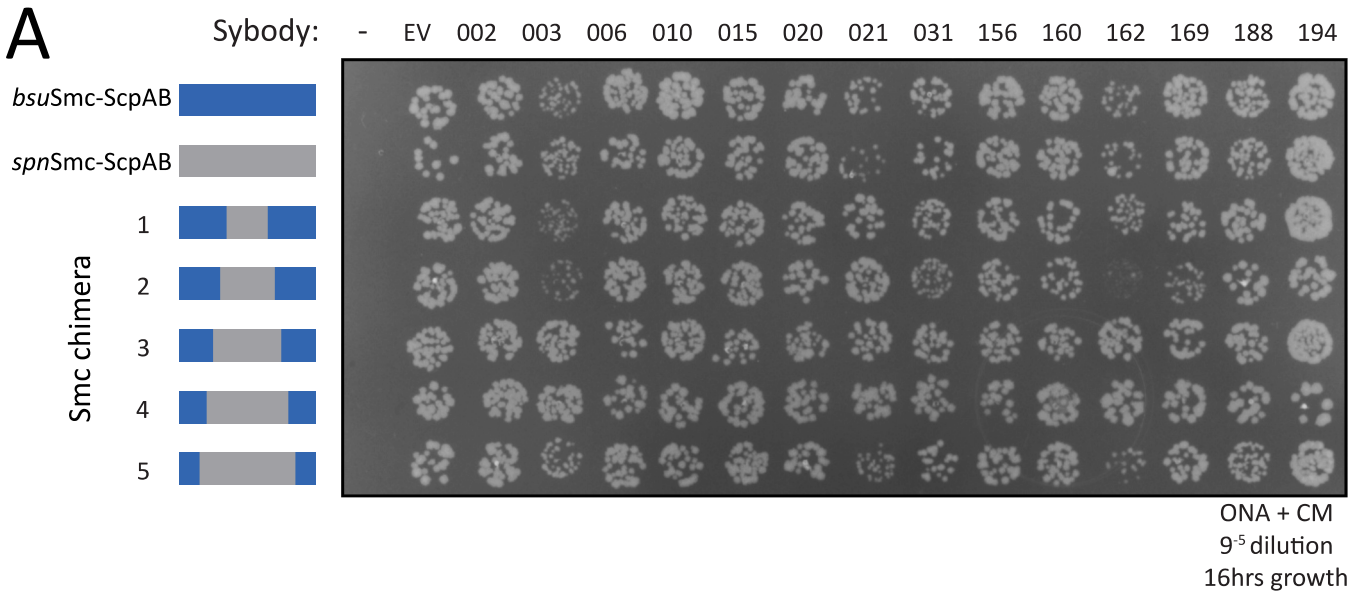
A
Sybody:
- EV 002 003 006 010 015 020 021 031 156 160 162 169 188 194
bsuSmc-ScpAB
spnSmc-ScpAB
Smc chimera
1
2
3
4
5
ONA + CM
9-5 dilution
16hrs growth

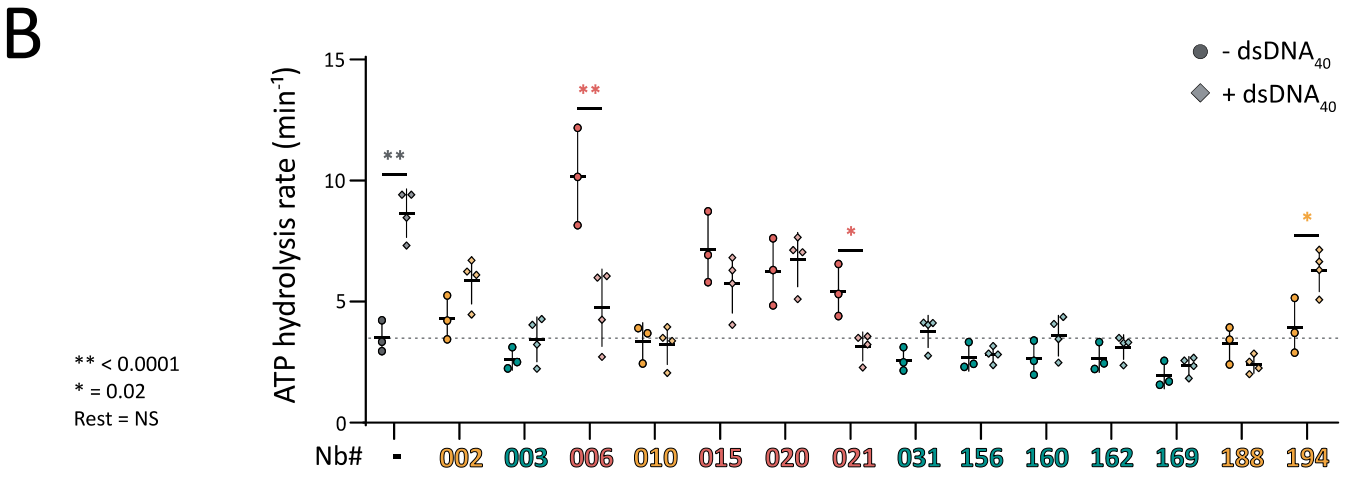
B
- dsDNA40
+ dsDNA40
ATP hydrolysis rate (min-1)
15
10
5
0
**
**
*
*
** < 0.0001
* = 0.02
Rest = NS
Nb#
-
002
003
006
010
015
020
021
031
156
160
162
169
188
194

Figure S6

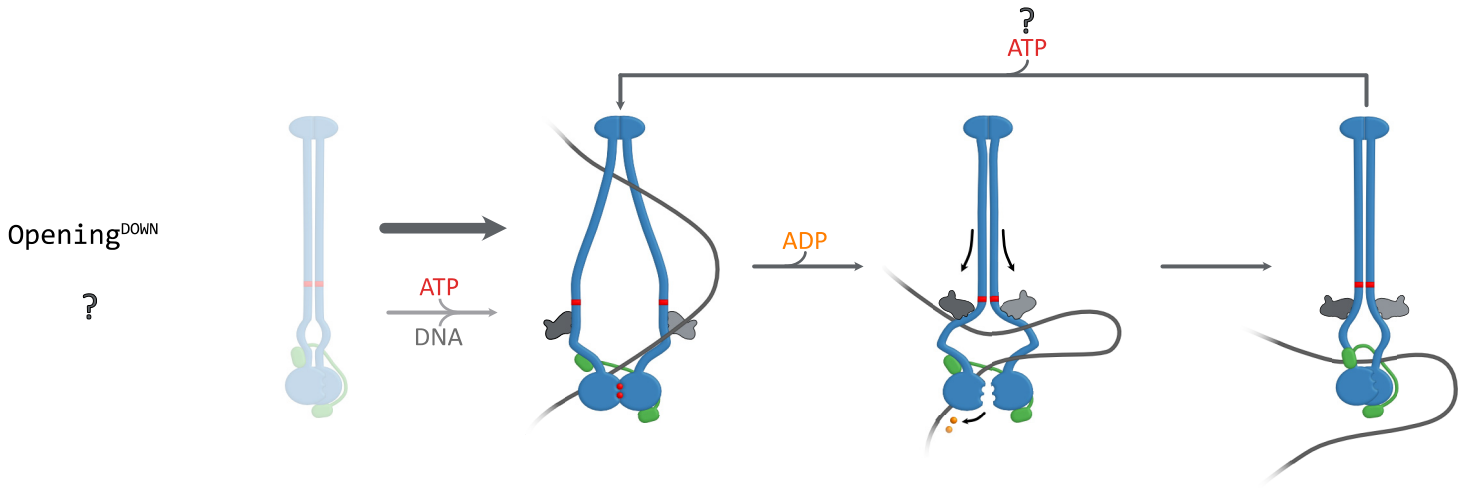

Figure S7